

# Politecnico di Torino

Master of Science in  
Electronic Engineering - Micro and Nanosystems

Master Thesis

## *Modeling of Spin Wave based Majority Gate*



POLITECNICO  
DI TORINO

imec

**Supervisor:**

*Prof. Fabrizio  
Giorgis*

**Author:**

*Rossella  
Stefanelli*

**Supervisor imec:**

*Dr. Christoph  
Adelmann*

October 2019

# Preface

I would like to thank my supervisors Christoph Adelman and Florin Ciubotaru for supporting me during the weekly meetings and for allowing me to know the world of spin waves. Then I want to thank my promoter Fabrizio Giorgis, for his time and his feedbacks. A special thank is for my family and Vincenzo, since they gave me every day the right encouragement. Last but not least I would like to thank my friends, for having been always present during this long journey.

# Abstract

The improvement of CMOS technology reaches some fundamental limitations. For this reason alternatives are necessary to overcome the scaling and performances issues of the standard electronics. One of these is spintronic, in particular the subgroup of magnonics, since its main advantage is the power efficient computation. Indeed these devices exploit the spin as information carrier, rather than the charge, hence there is no Joule heating. Furthermore magnonic devices allow wave computing with higher functionality than classic computing. The goal of this master thesis is to study the majority gate device with different operating mode: continuous and pulse regime. The modeling of the system is performed through micromagnetic simulations, hence it has been possible to characterize the spin waves behaviour, thanks to the computation of the fundamental parameters describing their propagation in this specific device (4). The obtained dispersion relations suggest that even if the waveguide is set on DE geometry, also BVW waves are present, because the system is non uniformly magnetized. As a consequence the majority gate is far from the ideal condition and this leads to important consequences on the performances of the device, as it will be explained in the chapter 5. Then the successive step is the study of the interference pattern if more than one inputs are applied. Relevant differences are found between the two operation regime (chapter 6). The pulse mode arouses particular interest, since usually an electronic device has to work with a clock scheme, hence the excitation applied has a limited duration. The computation efficiency changes depending on the shape of signal exploited as input. The Gaussian field is meant to offer the best performances, even if the goal of the research is to find an efficient operation mode applying rectangular pulses. From the comparison between Gaussian and rectangular excitation mode it has been found that in the second case more harmonics are present, as it is suggested by the Fourier Transform of the signal, leading to unwanted results.

# Contents

<b>1</b>	<b>Introduction</b>	<b>1</b>
<b>2</b>	<b>Theoretical Background</b>	<b>4</b>
2.1	Magnetization and Magnetic Moments . . . . .	4
2.2	Magnetostatic Energy Contributions . . . . .	7
2.2.1	Exchange Interaction . . . . .	7
2.2.2	Dipolar Interaction . . . . .	9
2.3	Dynamics in Ferromagnetism . . . . .	12
2.4	Spin Waves Behaviour . . . . .	14
2.4.1	Uniform Precession Mode . . . . .	15
2.4.2	Dipolar Spin Waves Mode . . . . .	16
2.4.3	Dipole-Exchange Spin Waves Mode . . . . .	18
2.4.4	BVW and DE Geometries . . . . .	20
2.4.5	Main Propagation Parameters . . . . .	21
<b>3</b>	<b>Simulation Setting and Procedures</b>	<b>23</b>
3.1	Waveguide Definition . . . . .	23
3.2	Software for Micromagnetic Simulations . . . . .	26
3.3	Ground State Computation . . . . .	27
3.4	External Excitation . . . . .	29
<b>4</b>	<b>Spin Waves Characterization in the Majority Gate</b>	<b>31</b>
4.1	Dispersion Relations . . . . .	31
4.2	Lifetime Computation . . . . .	34
4.3	Group Velocity Computation . . . . .	36
<b>5</b>	<b>Continuous Regime</b>	<b>39</b>
5.1	One Input Propagation Analysis . . . . .	40

## Contents

---

5.2	Interference Pattern Analysis . . . . .	44
5.2.1	Ideal Working Principle of Majority Gate . . . . .	45
5.2.2	Real Implementation of SWMG . . . . .	51
<b>6</b>	<b>Pulse Regime</b>	<b>53</b>
6.1	Gaussian Modulated Pulse with Carrying Frequency . . . . .	53
6.1.1	One Input Propagation Analysis . . . . .	56
6.1.2	Interference Pattern Analysis . . . . .	63
6.1.3	Shrinkage of the Gaussian Modulating Signal . . . . .	69
6.1.4	Repetition Rate . . . . .	71
6.2	Rectangular Pulse Excitation . . . . .	75
<b>7</b>	<b>Conclusion</b>	<b>81</b>

# List of Figures

1.1	The trident shaped majority gate is made by three parallel waveguides, which are the inputs, and then another waveguide representing the output. . . . .	3
1.2	In the "inline" structure the inputs and the output are placed in the same line; the substrate is $SiO_2$ . . . . .	3
2.1	If the $H_{eff}$ is applied to the magnetization vector a torque is produced. If the magnetic field changes in time, the precession motion is the consequence. . . . .	13
2.2	If all the spins are subjected to the dynamic field, they precess with a phase difference and a wave is produced. . . . .	13
3.1	The structure is divided in different areas: going towards the edge the damping value increases, in order to kill the reflections, in the region in the range $[-3 \text{ um}, 3\text{um}]$ (taking into account that the origin of the reference system is in the centre of the waveguide), the value of the damping is the lowest one. The reason why is because here the propagation of the spin waves has to take place. . . . .	25
3.2	The ground state magnetization is normalized respect to the saturation magnetization $M_s$ , and it plotted as a function of the width, in order to show the effects of the shape anisotropy. . . . .	27
3.3	The spins are oriented perpendicularly to the propagation direction (DE configuration), but at the edge shape anisotropy is present. . . . .	29
3.4	The compensation of demagnetization field allows to obtain a uniform ground state, without the shape anisotropy. . . . .	29

## List of Figures

---

3.5	The demagnetization field is plotted as a function of the width. The software Mumax3 put the origin of the coordinate system in the centre of the waveguide, hence the x axis has the range [-400 nm, 400 nm]. . . . .	30
4.1	Dispersion relations of the device: in the plot different curves are present. The numerical curve (dotted line) is obtained from the simulation, the analytic curves instead are obtained from the equation shown in chapter 2. . . . .	33
4.2	This plot represents the decay in time of the Fourier Transform of the k component equal to $6.29 \text{ rad}/\mu\text{m}$ . . . . .	35
4.3	Analytic lifetime is plotted for DE configuration mode 1; the external field considered is that one obtained from the compensation of the demagnetization field. . . . .	36
4.4	The group velocity corresponding to $k=6.29 \mu\text{m}$ is equal to: $3.23 \mu\text{m}/\text{ns}$ in the numerical case and $5.33 \mu\text{m}/\text{ns}$ in the analytic case. . . . .	38
5.1	The snapshot represents the component z of the magnetization and it is captured at $t=0.2 \text{ ns}$ . In the figure it is possible to see two irregularities at the left upper corner and the right bottom one: they are artifacts of simulation due to the geometry of the sample, that has to obey to the well known anisotropy law of magnetism. In the chapter 3 this phenomenon is clearly showed in the snapshot of the ground state. . . . .	40
5.2	The snapshot is taken at 0.5 ns. The intermediate waves become more relevant as the time flows, but far from the antenna the pattern is still the same as that one of the begin. . . . .	41
5.3	The snapshot is captured at 0.72 ns. It is clear that the pattern starts to change near the antenna, but as the time flows this change will propagate along all the waveguide if the simulation is long enough. . . . .	41
5.4	This snapshot is taken at 0.5 ns, hence in the same time of figure 5.2. In this case the red and blue line in $x=2\mu\text{m}$ , where antenna is placed and where intermediate waves start to propagate, are still separated if you look along y direction, instead in the other figure, in the same position, the red and blue line alternate along y direction. . . . .	42

## List of Figures

---

5.5	This plot represents the component $z$ of the magnetization in the space (along the $x$ direction) at a specific time (1.5 ns). It is clear that if the output is placed at a distance equal to a multiple of the wavelength the phase is equal to that of the input one. The output can be read only if the spin waves reached the output position, hence is very important the time at which the output has to be read. . . . .	44
5.6	The figure shows a snapshot of the simulation and it represents the case 0 1 0 illustrated in the table 5.2. In this case the interval time before reading the output is greater than other case because the first and second inputs are farther from the output, so they took more time to reach the output window. . . . .	47
5.7	In the case represented in this figure the distance between the three inputs is $n\lambda$ where $n=1$ . The phase is $\phi = 0$ : every signal has the same phase as the other inputs. Hence with these assumption also the output has the same phase of the inputs because there is a constructive interference among them. The snapshot is captured at $t \sim 0.6$ ns. . . . .	48
5.8	In the case represented in this figure the distance between the three inputs is $n\lambda$ where $n=1$ . The configuration of the inputs is equal to 0 1 0. The snapshot is captured at $t \sim 0.6$ ns. . . . .	48
5.9	The figure shows the component $z$ of the magnetization at the position $x=5 \mu m$ , where it is supposed to have the output, respect to the time. The two plots corresponds to the two configurations described so far. . . . .	49
5.10	The plots is obtained in function of the signal frequency used to excite the spin waves in the system. . . . .	52
6.1	This is the modulated signal composed by the sinusoidal (carrying) and Gaussian (modulating) ones. . . . .	54
6.2	The plot represents the Fourier Transform of the Gaussian pulse and then the modulated signal by Gaussian pulse. As it is clear from the picture the same Gaussian is centered in different frequency values in the two cases, but it is required to be centered on a specific frequency so the blue curve is better. . . . .	56

## List of Figures

---

- 6.3 The snapshots captured in this image include the interval time of the simulation that goes from 0.27 ns to 0.53 ns. They represent the evolution in time of the component  $z$  of the magnetization. . . . . 58
- 6.4 The signal is applied through the antenna at  $x = 2 \mu m$ , but the time spectrum of the spin waves and the spectrum of Fourier Transform are observed in space at different position. In particular the positions taken into account are  $x= 2\mu m$ ,  $x=4.2 \mu m$ ,  $x= 5.3\mu m$ . . . . . 59
- 6.5 The signal is applied through the antenna at  $x = 2 \mu m$ , then the Fourier Transform is performed at several time interval, in particular for  $t= 0.325$  ns (before reaching the maximum peak of the signal Gaussian shape),  $t=0.375$  ns (corresponding to the maximum peak of the signal),  $t= 0.475$  ns (near the end of signal, on the right side of the bell curve). . . . . 61
- 6.6 The two snapshots represents the uniform and the non uniform case. The first one has a scale for reduced magnetization, hence it is computed for unit length, instead the second one represents a non normalized magnetization so it has a different scale. But this doesn't matter, it's only a scale factor. They are captured in the same moment. . . . . 62
- 6.7 The snapshot is captured 0.7 ns in order to be sure that all the inputs reached the output. The configuration sent in the majority gate is 1 1 1, indeed the input are blue (1) and the output is also 1 (blue). . . . . 64
- 6.8 The plots represent the magnetization in time and the Fourier Transform at antennas position and at the output. In particular the points in the waveguide taken into account are: the first antenna ( $2 \mu m$ ), the third antenna ( $4.2 \mu m$ , far  $2 \lambda$  from the first input) and the output at  $5.3 \mu m$  ( $3 \lambda$  from the first antenna). . . . . 65
- 6.9 In the sketch the arrows represent the spin waves coming from a certain position. The marked line indicates a strong influence of a certain antenna on that one considered, instead a fine line indicates a lighter impact. . . . . 67

## List of Figures

---

6.10	The plot shows the average value in time of the magnetization at each antenna position and at the output. As it has been predicted, at $x=3.1 \mu m$ the intensity magnetization assumes the highest value, because this position is the only one that has the minimum distance from two antenna, rather than from one as it happens for the other points. In this case the configuration corresponds to 0 0 0. . . . .	68
6.11	In the figure is reported the magnetization in time at the output, resulting from the configuration 1 0 1. The zoom is done in the time window where the result is correct and it is in phase with the reference signal. . . . .	69
6.12	The magnetization in the plots is extracted at the output for both cases. The zoom shows the small shift between the two plots in the time interval where the output is correct. . . . .	70
6.13	The Fourier Transform has been performed for the normal and shrunken signal. The last one has the same parameter of the first signal, it changes only the value of the width, that determines the compression of the Gaussian modulation. . . . .	71
6.14	In the plot the two successive Gaussian modulated signal are shifted by a quantity equal to $\pi$ so they represents the two complementary bit values. . . . .	73
6.15	The reference signal has the same phase of value 0, this means that if the result of the operation is 0 it is in phase with the reference (first zoom), instead if the result of the input combination is 1 it is shifted respect to the reference of a quantity equal to $\pi$ (second zoom). . . . .	74
6.16	The Fourier Transform in space was computed in different moments: the blue curve corresponds to the time when only the first set generated spin waves are present, instead the orange curve corresponds to the time in which spin waves generated by the second set are present and interfere with the residual waves coming from the first set. . . . .	76
6.17	The plots represent the Fourier Transform of rectangular pulse with different width, in particular three values are present in the figure: $\sigma = 20ps, 50ps, 100ps$ . . . . .	77

## List of Figures

---

6.18	The output plotted represents the result of the 0 1 0 configuration. The reference signal has the phase of the value 0, hence it can be considered $\phi = 0$ , because in this dissertation this phase value has been assigned to the bit 0. . . . .	78
6.19	The plots represents the evolution in time of the component z of the magnetization, and the Fourier Transform in time at relevant positions: the first and third inputs and the output. .	79
6.20	In the plots the intensity of magnetization $m_z$ is represented as a function of time. The time window chosen on the x axis is corresponding to that one in which is possible to read the output. . . . .	80

# List of Tables

5.1	Taking into account $n$ inputs, the value of the output is false if $n/2$ or more arguments are false, and true otherwise. . . . .	45
5.2	For each combination of the inputs the distance between an input and the next one is indicated. . . . .	47
6.1	The table represents the simulation setting of inputs configuration for the two set of bits sent consecutively. . . . .	72

# Chapter 1

## Introduction

Complementary Metal Oxide Semiconductor devices (CMOS) devices have been exploited so far in order to perform logic operations. The electronics industry needs higher and higher performances in terms of computational speed and first of all in terms of scaling. Hence it is necessary to overcome the standard technology and to go beyond, indeed several CMOS alternative are proposed. One of these is spintronics: in this case the spin rather than the charge of electrons is exploited as information carrier [4]. In this dissertation magnonics, a subgroup of spintronics, is the main interest. The magnonic devices are based on spin waves, which consist in a collective excitation of the spins inside the magnetic material. Magnonic devices presents a great advantage with regard to the other spintronics devices: the characteristic propagation length of spin waves is much higher, because in the other case it is limited by the diffusion length of the spin polarized current [1].

The second advantage is the possibility of wave computing in magnonics, and this enhances the functionality for logic operations [2, 3, 5, 6]. The main problem of this devices is that they are still larger than CMOS, even if they give already promising results.

In magnonics, spin waves are exploited to transmit and process information in the magnetic materials. The information could be encoded in the phase or amplitude of the spin wave. These devices can compete with CMOS technology because they can exploit the wave properties and furthermore they are characterized by low power consumption. Spin waves have a wavelength in the nanometer range, if RF frequencies are used as exciting field, and this is much shorter than electromagnetic waves at the same frequencies [27]. This implies that the magnonics devices have a good scalability up to nanometer

range. Furthermore they solve current power issues because in this case there is no moving charge, hence there is no Joule heating. As a plus the interconnects become part of the logic, this is also another factor that contributes in the lowering of the power consumption [7, 8].

In this dissertation, one magnonic devices will be analyzed in particular: the majority gate. This device is implemented on a magnetic stripe (CoFeB) and three inputs are applied in order to perform the logic function. Over the decades an evolution occurred in the implementation of a majority gate through spin waves. The developed device is a majority gate for some specific reason: it allows the evaluation of the majority of an odd number of input signals, and furthermore it allows also the computation of AND and OR operations if one input is kept constant as control input. Thereby the advantage of the majority gate is its functionality and its configurability [9]. The working principle of the magnonic majority gate is based on the interference occurring at the output among the applied inputs. The information about the result of the logic operation is carried in the phase or in the amplitude of the spin wave at the output window: it is given by the superposition of all spin waves generated starting from the inputs. The geometry of the structure is fundamental in determining the behaviour of spin waves during propagation. In the past "trident" shape (figure 1.1) has been exploited in order to implement the majority function. According to this method the three input are placed in three different waveguide parallel to each other, and then the three signals interact at the junction point of the three arms, realizing the interference and providing the result of the gate. The main problem of this geometry is the reflection at the bending of the structure, and the situation get worse when the system is scaled. The evolution is the sequential "inline" layout of input and output, figure 1.2 [10]. In this last case there is only one waveguide, which host input windows at a specific distance between two successive inputs, and in the end there is the output window, where the result of the interference among three inputs is read and brought to the external world.

In more detail the object of this study is to obtain more understanding of the working of the majority gate in continuous regime and in pulse regime. First of all spin waves characteristics in the majority gate are analyzed. To reach the goal dispersion relations, lifetime, group velocity and decay length are computed, comparing the results in two different case: uniformly magnetized waveguide and non uniformly magnetized waveguide. This is useful for understanding the limitation of the device due to the internal demagnetizing

field. Furthermore through the study of the dispersion relation it is possible to know which type of spin waves are present in the waveguide and which are their propagation modes. Micromagnetic simulation are performed in order to obtain the evolution in time of the spin waves inside the waveguide.

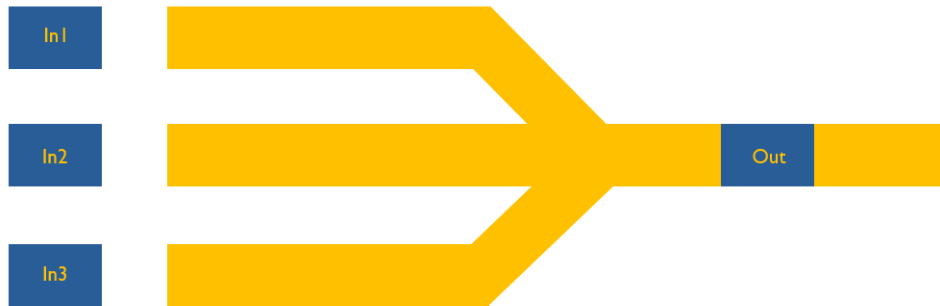


Figure 1.1: The trident shaped majority gate is made by three parallel waveguides, which are the inputs, and then another waveguide representing the output.

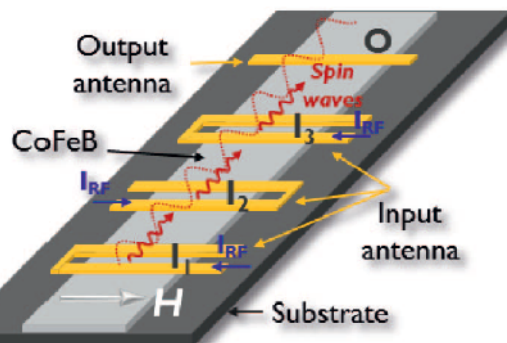


Figure 1.2: In the "inline" structure the inputs and the output are placed in the same line; the substrate is  $SiO_2$ .

# Chapter 2

## Theoretical Background

In the field of spin waves ferromagnetic materials are exploited. The peculiarity of ferromagnetic materials is that they are composed by different microscopic regions called magnetic domains. If no external field is applied each domain is random oriented, hence the net magnetization is very low. Instead when magnetic field is applied, they align in the same direction of the applied field, hence now the net magnetization is relevant. In the following sections the most important concepts about ferromagnetism will be treated in order to explain the basic mechanisms of spin waves [4].

### 2.1 Magnetization and Magnetic Moments

Ferromagnetic materials consist of atoms made up of electric charges. The charges in the atomic cloud have an angular momentum from which the magnetic moment is generated. The relation between the magnetic moment and the angular momentum is:

$$\mu = \gamma J \tag{2.1}$$

where  $\gamma$  is the gyromagnetic ratio which equals to:

$$\gamma = \frac{q}{2m} \tag{2.2}$$

where  $q$  represents the electric charge, instead  $m$  is the mass of the magnetic

dipole. In the atom two different type of angular momentum are present: the orbital angular momentum  $\mathbf{L}$  (essentially due to the motion of electron around the nucleus) and the spin angular momentum  $\mathbf{S}$  (this is an intrinsic property of the electron). The two angular momentum yield two type of magnetic moment [27, 4]:

$$\begin{aligned}\mu_L &= -\frac{\mu_B}{\hbar}\mathbf{L} \\ \mu_S &= -\frac{g_e\mu_B}{\hbar}\mathbf{S}\end{aligned}\tag{2.3}$$

where  $g_e$  is the Landè factor, which could be approximated by 2 for free electrons. Instead  $\mu_B$  is the Bohr magneton, representing the quantum of a magnetic dipole of an electron and it is equal to  $\frac{e\hbar}{2m}$ .

If the orbital and spin angular momenta are independent each other, the two contributions can be summed, indeed the total magnetic moment of the electron is equal to  $\mu_J = \mu_L + \mu_S$ . This condition is called Russell-Saunders coupling and it is valid only if there is no interaction between the orbital angular momentum and the spin angular momentum. Hence this means that the interaction between two spins is much stronger than the interaction between the orbital and the spin. It occurs when the external applied field is weak, since in this situation the spin-orbit interaction is weak. In other case where this interaction cannot be neglected anymore, another relation is suitable for computing the total magnetic moment of an electron:

$$\mu_J = -\frac{g_J\mu_B}{\hbar}\mathbf{J}\tag{2.4}$$

where  $\mathbf{J}$  is the total angular momentum and  $g_J$  is given by:

$$g_J = \frac{3S(S+1) - L(L+1)}{2J(J+1)}\tag{2.5}$$

Through these equation the magnetic moment of the electron is obtained, but in order to obtain the total magnetic moment of the atom it is necessary to compute the vectorial sum of the magnetic moments of all the electrons inside the atom. Since the completely filled shells have the same number of spins up and spins down, in this case the total net magnetic moment is equal to zero. Hence only the valence shell can contribute to the total magnetic moment of the atom, which is represented by the following relation:

$$\mu_{atom} = -\frac{gJ\mu_B}{\hbar} \sum_i (L_i + S_i) \quad (2.6)$$

with the sum performed on the all valence electrons in the atom. Furthermore the magnetic moment of a ferromagnetic material, formed bringing together several atoms, intuitively is given by the vectorial sum of the magnetic moments of each atom, hence the total magnetic moment is equal to:

$$\mu_{tot} = \sum_i \mu_{atom,i} \quad (2.7)$$

Despite this method to find the total magnetic moment is valid, it is more useful to deal with a continuous vector field in order to describe the behaviour of a ferromagnetic material, rather than taking into account single atomic dipoles. This field corresponds to the magnetization field, and it represents the amount of magnetic dipoles per unit of volume:

$$M = \frac{\sum_i \mu_i}{\delta V} \quad (2.8)$$

The normalized magnetization is a parameter largely exploited in order to have a better comparison among different ferromagnetic materials. It is equal to  $m = \frac{M}{M_s}$  where  $M_s$  represents the saturation magnetization. Physically speaking the magnetization of a ferromagnetic material corresponds to the magnetic field  $B$  created by the magnetizing field  $H$  externally applied. The magnetization extends out of the material, and this magnetic flux density is as higher as the applied field increases. If one has a look on the hysteresis curve of the material, it is possible to see that a certain point the value of the magnetization reaches a saturation condition and the corresponding value is the saturation magnetization. When the material reaches this condition the magnetization is still increasing, but at a paramagnetic rate, which is slower than ferromagnetic one.

The material analysed in the simulations is the CoFeB: in this case the magnetic properties are mainly determined by the spin angular momentum rather than the orbital one [27].

## 2.2 Magnetostatic Energy Contributions

The ferromagnetic material considered in this work is supposed to have a static magnetization state, this means constant in time. Every state has determined energy contributions, hence a energy function is necessary to describe the evolution in the magnetization state. This function is the Gibbs free energy and it is influenced by different contributions. Each energy contributions provides a corresponding effective magnetic field.

### 2.2.1 Exchange Interaction

The exchange interaction determines if the material is diamagnetic, paramagnetic or ferromagnetic. The interaction is determined by the orbital overlap of the electrons. Electrons are fermions, thereby they obey to Pauli exclusion principle. Taking into account this fact it is possible to describe the total exchange energy of spin  $i$ , in a system composed by  $N$  atoms, by exploiting the Heisenberg model [27]:

$$\epsilon_{ex} = -2 \sum_{j \neq i}^N \mathcal{J}_{ij} S_i \cdot S_j \quad (2.9)$$

where  $S_i$  and  $S_j$  are the spins on atom  $i$  and  $j$ , instead  $i_{ij}$  is the overlap integral between the two atoms. This energy is computed between the atom  $i$  and all other atoms different from  $i$ . The energy has a fast decaying behaviour since the overlap and the interaction drop if the atom taking into account are far from each other. Hence the previous relation can be limited only to the neighboring atom. In order to have the total exchange energy over the entire magnetic system it is necessary to perform the above computation for every atom [27]:

$$E_{ex} = -2 \sum_i^N \sum_{j \neq i}^N \mathcal{J}_{ij} S_i \cdot S_j \quad (2.10)$$

Depending on the sign of the overlap integral, it is possible to define different kind of material. If the integral is positive, the situation is called ferromagnetism, otherwise it will be antiferromagnetism condition. In the third case,

the thermal energy could be greater than the exchange energy. This means that magnetic order is lost and no net magnetization could exist without an external field, hence the material is paramagnetic.

At this point it is necessary to obtain the effective magnetic field generated by this interaction. In order to simplify the computation, an approximation is used. If the amplitude is the same for all the spins, and furthermore the misalignment between the spins is small, the dot product  $S_i \cdot S_j$  can be approximated to the second order of the Maclaurin series:

$$S_i \cdot S_j = S^2 \left[ 1 - \frac{1}{2} (r_{ij} \cdot \nabla m(r_{ij}))^2 \right] \quad (2.11)$$

with  $r_{ij}$  is the distance between the spins  $i$  and  $j$ , instead  $m$  is the normalized magnetization.

If a substitution is performed (2.11 in 2.10) and if isotropic media is assumed ( $\mathcal{J}_{ij} = \mathcal{J}$ ), the following relation is provided:

$$\epsilon_{ex} = -2\mathcal{J}S^2 + \mathcal{J}S^2 \sum_{j \neq i} (r_{ij} \cdot \nabla m(r_{ij}))^2 = -2\mathcal{J}S^2 + A_{ex} \int \nabla m(r)^2 dr \quad (2.12)$$

In the last step the sum can be replaced by the integral only if the lattice parameter is small regarding to the variation of magnetization in space.  $A_{ex}$  is the crystallography dependent exchange stiffness constant and it is equal to [11]:

$$A_{ex} = \frac{n\mathcal{J}S^2}{a} \quad (2.13)$$

where  $a$  is the lattice constant,  $S$  is the magnitude of the spin and  $n$  depends on the symmetry of the crystal system. In the simulation performed in this work the exchange stiffness constant is in the order of magnitude of  $10^{-11}$  J/m.

In order to obtain the effective field yielded by the exchange interaction, the following relation is used [27]:

$$H_{eff} = -\frac{1}{\mu_0 M_s} \frac{\partial \epsilon(m)}{\partial m} \quad (2.14)$$

with  $\mu_0$  vacuum permeability,  $M_s$  is the saturation magnetization and  $\epsilon$  is the energy computed in 2.12. This field is not a real quantity, but it is only a

mathematical representation in order to describe some quantum mechanical effects. The exchange length is another parameter that allow to compute how strong is the exchange interaction with regard to the dipolar interaction [28, 27]:

$$l_{ex} = \sqrt{\frac{2A_{ex}}{\mu_0 M_s^2}} \quad (2.15)$$

This quantity will be exploited to determine the size of the cell in the sample under test in the simulation (chapter 3).

## 2.2.2 Dipolar Interaction

The dipolar interaction concerns two different type of interaction because the dipoles can react to an externally applied field, but also to the own magnetic field of the material.

### Zeeman Energy

If an external field is applied on a system composed by  $N$  magnetic dipoles the energy resulting from the interaction is equal to:

$$E_{ex} = -\mu_0 \sum_{i=1}^N H_{ext} \cdot \mu_i \quad (2.16)$$

Looking at the relation 2.16 it is possible to recognize in the sum the total magnetization of the system per unit volume, indeed the energy density function is equal to:

$$\epsilon_{ext} = -\mu_0 H_{ext} \cdot M \quad (2.17)$$

If the magnetization is parallel to the external field the system is in the minimal energy state, instead if they are antiparallel the system is the maximum energy state.

### Demagnetization Field

The magnetic dipole in a material not only react to an external magnetic field, but they provides themselves a magnetic field according to the equation below [29]:

$$H_{d,i} = \frac{1}{4\pi} \left( \frac{3r(r \cdot \mu_i)}{|r|^5} - \frac{\mu_i}{|r|^3} - \frac{4\pi}{3} \frac{\mu_i}{\delta(r)} \right) \quad (2.18)$$

In 2.18  $H_{d,i}$  is the magnetic field yields by one single dipole, instead  $r$  is the distance between a random point in the space of the system and the magnetic dipole taken into account.

If another dipole is placed in this space there will be a certain interaction between the dipoles present, and the consequent energy is equal to [30]:

$$E_d = \frac{\mu_i \cdot \mu_j}{r_{ij}^3} - 3 \frac{(\mu_i \cdot r_{ij})(\mu_j \cdot r_{ij})}{r_{ij}^5} \quad (2.19)$$

$E_d$  is generated by the interaction of the dipoles  $\mu_i$  and  $\mu_j$ , instead  $r_{ij}$  is the distance between them. In 2.19 only the interaction between two dipoles has been taken into account, but if more dipoles enter in the analysis of the system the relation becomes more complex. The total demagnetizing field is given by the sum of all contributions among different dipoles, considering the full set of combination among dipoles. This field is present both in and outside the material, and that one in the material is called demagnetization field. This field yields an increase in the interaction energy of the system, but it is weaker than the exchange energy. Despite this fact the demagnetizing one is a long-range interaction, hence it is more relevant in the total magnetostatic energy of the material.

The demagnetizing field can be computed with different methods. One consist in solving the Maxwell's equation [27]:

$$\begin{aligned} \nabla \cdot B &= \nabla \cdot \mu_0(H + M) = 0 \\ &\rightarrow \nabla \cdot M = -\nabla \cdot H \end{aligned} \quad (2.20)$$

It is a differential equation so boundary conditions are necessary:

$$\begin{aligned} H_{\parallel,in} &= H_{\parallel,out} \\ B_{\perp,in} &= B_{\perp,out} \end{aligned} \quad (2.21)$$

Regarding the boundary conditions,  $H$  is referred to the field parallel to the interface of the material, instead  $B$  is the magnetic induction perpendicular to the surface. Exploiting this boundary conditions, then it is possible to obtain the demagnetizing field.

Another method to compute the demagnetization field is through the magnetization:

$$H_{demag} = -\hat{N}M \quad (2.22)$$

where  $\hat{N}$  is the demagnetization tensor and it depends on the shape and on the position in the sample. However in the case of an ellipsoid the demagnetization field and the magnetization are uniform. Usually the tensor  $\hat{N}$  is a general matrix but in the case of an ellipsoid it is a diagonal matrix and  $\hat{N}$  is not position dependent. If 2.14 is exploited with 2.22 it is possible to obtain the density energy function corresponding to the demagnetizing field:

$$\begin{aligned} \epsilon_d &= \frac{1}{2}\mu_0(N_{xx}M_x^2 + N_{yy}M_y^2 + N_{zz}M_z^2) \\ \mathcal{E}_d &= \frac{1}{2}\mu_0V(N_{xx}M_x^2 + N_{yy}M_y^2 + N_{zz}M_z^2) \end{aligned} \quad (2.23)$$

In the case of an ellipsoid the total energy due to the demagnetizing field is not given by an integral on the volume, since the magnetization and the demagnetization are uniform, thereby all computation is reduced to the multiplication.

The demagnetization field is generated by the surface poles which provide a magnetic field perpendicular to the surface. According to 2.17 the minimal energy state is achieved when the magnetization and the magnetic field are aligned. Furthermore from 2.22 one can see that demagnetizing field always opposes to the magnetization, because of the minus sign. This means that in order to have the minimal energy state it is necessary to reduce the number of surface poles (pole avoidance principle), and consequently also the demagnetizing field. For this purpose the surface poles try to align in the direction of the longest dimension: indeed in this way the plane perpendicular to this direction has the smallest surface, and the number of poles is lower. Mathematically speaking this means that  $\hat{N}$  has small values for long axis direction. Furthermore the demagnetization field is strongly dependent on the geometry of the sample, as it is suggested by the pole avoidance principle. This

phenomenon is called shape anisotropy and it becomes more relevant as the sample is scaled down, indeed the magnetization and the energy will change. Shape anisotropy is not the only one, because in the case in which the sample has a crystallographic structure, magnetocrystalline anisotropy arises. This kind of anisotropy originates from the spin-orbit coupling of the electrons, that makes energy related to spin orientation no longer isotropic. In this work the magnetocrystalline anisotropy is not taken into account because the material is polycrystalline and this leads to isotropic properties in the material.

## 2.3 Dynamics in Ferromagnetism

So far the different energetic contributions are analyzed. According to the equation 2.14, the energy variation in time yields an additional components in the field. Hence the total effective magnetic field present in the material is given by the sum of all fields [4, 27]:

$$H_{eff} = H_{ex} + H_{ext} + H_{demag} \quad (2.24)$$

If a dipole is subjected to this effective field, the dipole will try to align with the field, in order to reach the minimal state of energy. If the dipole is not aligned a momentum will be exerted according to the following relation (figure 2.1, [13]):

$$\tau = \mu_0(\boldsymbol{\mu} \times H_{eff}) \quad (2.25)$$

The torque tries to align the magnetic dipole with the magnetic field, in order to achieve the more stable energy configuration. Taking into the Newton's second law, according to which the torque corresponds to a variation in time of the angular momentum one can obtain:

$$\frac{d\boldsymbol{\mu}}{dt} = \gamma\mu_0(\boldsymbol{\mu} \times H_{eff}) \quad (2.26)$$

In this equation a single dipole is taken into account, but if a magnetic material is the subject of the analysis it is better talking about a collective of

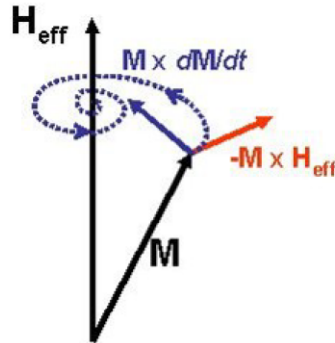


Figure 2.1: If the  $H_{eff}$  is applied to the magnetization vector a torque is produced. If the magnetic field changes in time, the precession motion is the consequence.

single dipoles, that are present in the volume occupied by the sample. Hence the relation 2.26 is transformed in the following:

$$\frac{d \sum_i \mu_i}{dt} = \gamma \mu_0 \left( \sum_i \mu_i \times H_{eff} \right) \quad (2.27)$$

In this case it is convenient exploiting the concept of magnetization field, rather than using the sum of single dipoles. In the end one obtains the Landau-Lifshitz equation 2.2, [13]:

$$\frac{dM}{dt} = \gamma \mu_0 (M \times H_{eff}) \quad (2.28)$$

If a torque is exerted on the dipoles because the magnetization is not aligned

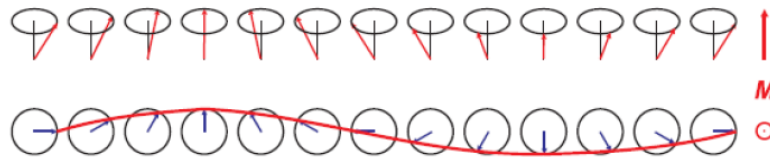


Figure 2.2: If all the spins are subjected to the dynamic field, they precess with a phase difference and a wave is produced.

with the magnetic field, the magnetization vector starts to precess with a certain frequency given by the formula:

$$f_L = \frac{|\gamma|\mu_0 H_{eff}}{2\pi} \quad (2.29)$$

The precession frequency is called Larmor frequency [27]. Generally speaking, in the equation 2.28 damping is not taken into account, hence ideally the magnetization should precess forever, if the magnetic field is stationary. But it is necessary to include damping in the equation, because after a certain time interval the magnetization reaches an equilibrium condition and it is aligned with the magnetic field. The damping phenomenon is caused by different effects, such as magnon-magnon scattering or magnon-phonon scattering or eddy currents [12]. In order to take into account this factor influencing the magnetization, an additional term in the equation 2.28 is required. It is very hard to mathematically describe this phenomenon, hence a dimensionless constant  $\alpha$  is introduced. Hence the modified formula is called Landau-Lifshitz-Gilbert equation [27]:

$$\frac{dM}{dt} = \gamma\mu_0(M \times H_{eff}) + \frac{\alpha}{M_s}M \times \frac{dM}{dt} \quad (2.30)$$

The effect of the damping does not influence the speed of the precession and the Larmor frequency is the same. The consequence of the damping is to attenuate the precession until an equilibrium state is reached and the magnetization is aligned to the effective field. This happens if the magnetic field is stationary in time, instead if the field varies in time the magnetization never reaches the equilibrium condition. The concept will be explained in detail talking about the spin waves [27, 4].

## 2.4 Spin Waves Behaviour

As already explained in the previous section, the spin waves arise when the effective field is time-varying, hence the magnetization vector never reaches an equilibrium state, and the precession keeps going because the alignment between the magnetization and the effective field is never realized. Even if

the equilibrium is not possible, a steady state can be reached: in this condition all the spins precess with the same frequency and the same amplitude, but with different phase. The steady state is defined by the fact that magnetic energies remains constant in time, even if it is higher than in the ground state.

Mathematically speaking this corresponds to a wave behaviour, hence in a magnetic material spin waves are defined. The propagation of these waves is related to the fact that the deviation from the equilibrium state is not confined in a specific site, but it is distributed to all the spins in the crystal [27]. The spin waves can be defined as a collective excitation of magnetic moments [13]. These waves can be described also through their quasiparticle called magnon, corresponding to the quantum of a spin wave. The magnon is defined as the region where there is an high probability to have flipped spins. Since magnons are bosons, in the same region more than one spins can be flipped. In the following paragraphs a detailed description of spin waves will be reported.

### 2.4.1 Uniform Precession Mode

There are a certain range of frequencies for which the spin waves can be well excited in a specific geometry. Furthermore if the Larmor frequency, determined by the effective magnetic field, is equal to the FMR (ferromagnetic resonance), the precessional motion has the same phase for all the spins in the material. Intuitively it is possible to attribute to these spin waves an infinite wavelength [4].

In the FMR condition it is possible to describe the magnetization and the effective magnetic field in this way:

$$\begin{aligned} H_{eff}(t) &= H_0 \hat{z} + h e^{i\omega t} \\ M(t) &= M_0 \hat{z} + m e^{i\omega t} \end{aligned} \tag{2.31}$$

Here  $M_0$  and  $H_0$  are the static magnetization and the static external field, instead  $h$  and  $m$  are dynamic components. It is possible to obtain the FMR frequency from the LLG equation, for an unbounded medium: this means that the effective field corresponds totally with the external field, since in this case the other contributes are negligible. If it is supposed that  $|h| \ll H_0$

and  $|m| \ll M_0 \approx M_s$ , one can obtain a linearized LLG equation that yields a linear relationship between the dynamic components of the magnetization and the field [27]:

$$m = \hat{P}h \quad (2.32)$$

$$\hat{P} = \begin{pmatrix} \chi & ik & 0 \\ -ik & \chi & 0 \\ 0 & 0 & 0 \end{pmatrix} \quad (2.33)$$

$$\chi = \frac{\omega_H \omega_M}{\omega_H^2 - \omega^2} \quad (2.34)$$

$$k = \frac{\omega_M \omega}{\omega_H^2 - \omega^2} \quad (2.35)$$

$\hat{P}$  is the Polder susceptibility tensor,  $\omega_M = \gamma\mu_0 M_s$  and  $\omega = \gamma\mu_0 H_0$ . The resonance condition occurs when the denominator of  $\chi$  goes to zero, this means that  $\omega = \omega_H$ , and this condition the dynamic magnetization reaches theoretically an infinite value: this corresponds to the resonance.

When a bounded ellipsoidal medium is taken into account, it is necessary to include the demagnetization field, hence  $H_{eff} = H_{ext} + H_{demag}$ . Now exploiting the linearized LLG equation one obtains the Kittel equation [14]:

$$f_{res,ellipsoid} = \frac{\gamma\mu_0}{2\pi} \sqrt{(H_0 + (N_{yy} - N_{zz})M_s)(H_0 + (N_{xx} - N_{zz})M_s)} \quad (2.36)$$

Also in 2.36 the approximation is valid only if the dynamic components are much smaller than the static ones.

### 2.4.2 Dipolar Spin Waves Mode

In the previous section one particular case has been taken into account: all the spins precess with the same phase. If now it is supposed that non uniform excitation field is introduced in the system, the wavelength is finite hence  $k \neq 0$ . The dynamic components of the magnetization and the field must be rewritten as follows:

$$\begin{aligned}\mathbf{h}(r, t) &= \mathbf{h}e^{i(k \cdot r - \omega t)} \\ \mathbf{m}(r, t) &= \mathbf{m}e^{i(k \cdot r - \omega t)}\end{aligned}\tag{2.37}$$

As one can observe from the equation, in this case there is an oscillation in time and in space. In the formulation of dipolar waves it is supposed that the dipolar field is much larger than the exchange field, hence the wavelength is much larger than the exchange length. In order to obtain the mathematical description of these waves it is necessary to exploit the Maxwell equations for determining the magnetic field, and the LLG equation for determining the magnetization vector. Since electromagnetic waves in a magnetic material are slower than electromagnetic waves in the air, it is possible to neglect the dynamic part of Maxwell's equation. As a consequence the magnetic and electric field are fully decoupled. This means that the magnetostatic approximation is applied [27]. The main advantage of spin waves based devices is that electromagnetic waves in magnetic material have shorter wavelength than wave in the air, this means that it is possible to build smaller structure, hence spin waves are suitable for the scaling of the technology. Thanks to the magnetostatic approximation it is possible to describe the magnetization in space, combining the Maxwell's equations in one. In order to achieve the final formulation, a new quantity needs to be defined, which is the magnetic potential  $\phi$ :

$$h = -\nabla\phi\tag{2.38}$$

Then taking into account the relationship between  $\mathbf{b}$  (magnetic induction) and  $\mathbf{h}$  (magnetic field):

$$\mathbf{b} = \hat{\mu}\mathbf{h} = (\hat{I} + \hat{\chi})\mathbf{h}\tag{2.39}$$

where  $\hat{I}$  and  $\hat{\chi}$  are respectively the identity tensor and the susceptibility tensor. Now one can obtain the Walker equation [27] if equations 2.38 and 2.39 are combined with the magnetostatic equations:

$$(1 + \chi) \left[ \frac{\partial\phi^2}{\partial x^2} + \frac{\partial\phi^2}{\partial y^2} \right] + \frac{\partial\phi^2}{\partial z^2} = 0\tag{2.40}$$

Through this method dispersion relation and magnetization components in time and space are yielded. In particular the Walker equation allows to obtain the dipolar field, then it is used in the LLG equation to compute the magnetization variation in time. The Walker equation and the LLG equation are complementary because the first one takes the magnetization in a specific moment in time and calculates the dipolar field, instead the second one takes the obtained dipolar field to obtain the magnetization behaviour in time.

In the magnetostatic limit the spin waves are fully degenerate, this means that for a certain frequency exist an infinite number of wavenumbers. If exchange interaction and dimensional confinement are introduced, the degeneracy is overcome.

### 2.4.3 Dipole-Exchange Spin Waves Mode

It is possible to distinguish three different regime. At long wavelengths ( $l_{ex}k \ll 1$ ) dipolar waves are dominant, instead at short wavelengths ( $l_{ex}k \gg 1$ ) exchange waves are present. In between these two limits spin waves are characterized by dipole-exchange regime. In the regime described so far, different kinds of interaction occurs: in the dipolar waves case electric and magnetic interaction is more important respect to the exchange one; for magnetostatic waves electric and exchange interaction are both negligible respect to the magnetic one; in the last case exchange interaction is the most important one.

Generally speaking the spin waves regime occurs when the magnetization is out of equilibrium, and the excited state has dynamic magnetization components in resonance. The most efficient way to describe spin waves characteristics is through the dispersion relations  $\omega(k)$ . The formula for dispersion relations changes depending on the geometry of the system.

For an unbounded medium, the dispersion relation is defined by the Herring-Kittel equation [27]:

$$\omega = \sqrt{(\omega_H + \omega_M \lambda_{ex} k^2)[\omega_H + \omega_M(\lambda_{ex} k^2 + \sin^2(\theta))]} \quad (2.41)$$

If the media is unbounded the static internal field corresponds to the static external field. Furthermore  $\theta$  is the angle between the wave vector and the

static field, instead  $\lambda_{ex} = l_{ex}$ .

From the equation 2.41 one can deduce that the exchange interaction increases the resonance frequency. If the wave vector is small, dipolar regime occurs hence the dispersion relation can be approximated to:

$$\lim_{k \rightarrow 0} \omega \approx \sqrt{\omega_H(\omega_H + \omega_M \sin^2(\theta))} \quad (2.42)$$

Instead when  $k$  is large, spin waves are in the exchange regime:

$$\lim_{k \rightarrow \infty} \omega \approx \omega_M \lambda_{ex} k^2 \quad (2.43)$$

As it is clear from the approximated relations obtained above, the anisotropy is a consequence of the dipolar interaction, indeed only in the dipolar regime one can notice a dependence from the magnetization orientation (in the dispersion relation a dependence from  $\theta$  appears).

The Herring-Kittel equation describe only dispersion relation in the case an unbounded medium, but in the case of the device studied in this dissertation the system is bounded, hence it is necessary to introduce boundary conditions and confinement in the mathematical derivation.

The main interest in the case of the subject analyzed here is regarding the dispersion relations in a small magnetic waveguide. Hence the spin waves are confined in a one dimensional structure, and the beam is confined in the length  $l$ , the width  $w$  and height  $d$ . The confinement is in two dimension (width and height), thereby the wave vector is considered quantized only in these two dimensions. It is assumed that a small waveguide has a small thickness, hence one can assume that it is present only the zero order thickness mode  $m=0$ . This phenomenon happens because the second order thickness mode appears at higher frequencies. In this condition the spin waves have the same amplitude for the entire thickness, hence if over the thickness is a constant it is possible to consider the mode profile along the width direction taking into account the narrow waveguides. Even if the lateral quantized wave vector depends on the boundary conditions, if the width is much larger than the thickness, the lateral wave vector can be approximated by:  $k_n = \frac{n\pi}{w}$ , where  $n$  is an integer number [15]. At this point one can deduce that the total wave vector has to be written as:  $k_{tot} = k + k_n$ , where  $k$  is referred to the length direction, instead  $k_n$  recalls the wave vector in the width direction. Exploiting the perturbation theory with specific boundary conditions

and supposing that the surface is unpinned (surface spins are fully free to move), one can obtain the dispersion relations [16]:

$$\omega_n = \sqrt{(\omega_H + \omega_M \lambda_{ex} k_{tot}^2)(\omega_H + \omega_M \lambda_{ex} k_{tot}^2 + \omega_M F)} \quad (2.44)$$

$$F = 1 - g \cos \theta_k - \theta_M^2 + \frac{\omega_M g (1 - g) \sin \theta_k - \theta_M^2}{\omega_H + \omega_M \lambda_{ex} k_{tot}^2} \quad (2.45)$$

$$g = 1 - \frac{1 - e^{dk_{tot}}}{dk_{tot}} \quad (2.46)$$

Here  $\theta_k = \arctan(\frac{k_x}{k})$ , instead  $\theta_M$  is the angle between the magnetization and the length direction of the structure. As one can notice from the equation 2.44, there are different modes depending on the number  $n$ , and each mode has its own dispersion relation, and the waveform corresponding to that specific mode can be defined as:

$$m_z^n(x, y, t) \sim \cos(k_n y) e^{i(kx - \omega(k)t)} \quad (2.47)$$

where  $\hat{x}$  represents the longitudinal direction,  $\hat{y}$  represents the width direction, hence it is perpendicular to the propagation direction but it is still in plane, and  $\hat{z}$  is the out of plane direction.

The dispersion relations obtained so far are valid only for uniformly magnetized waveguide.

#### 2.4.4 BVW and DE Geometries

Backward volume waves geometry is realized when the magnetization is parallel to the propagation direction (the longitudinal one). In this condition the demagnetization field is approximately zero, since all the spins are magnetized in the same direction and non uniformity doesn't occur at the edge. Hence in this case the static internal field is the same as the external applied field. When spin waves are excited also dynamic components of the field are present, not only the static ones. Furthermore the dynamic field has not the same direction as the longitudinal one, hence a demagnetization field is created. Because of the inhomogeneity of this field a dipolar pinning is created at the edge of the structure, and this not due to the magnetic anisotropy.

The second kind of geometry is Damon-Eschbach (DE), which is characteristic of the surface waves. In this case the magnetization is perpendicular to the propagation direction, but it is still in-plane. For DE geometry there are no different thickness modes [27]. If the structure is thick the waves are decaying away from the surface, instead if the waveguide is thin the intensity of the magnetization can be considered constant across the thickness. In this case differently from the BVW waves, also the width influences the magnetization. Indeed if the structure becomes very small, the demagnetization field increases, hence the static internal field is subjected to a strong reduction. With these assumptions one can define the effective static internal field [17]:

$$H_{eff}(y) = H_{ext} - \frac{M_s}{\pi} \left( \arctan \left( \frac{d}{2y+w} \right) - \arctan \left( \frac{d}{2y-w} \right) \right) \quad (2.48)$$

In this kind of geometry static internal field is position dependent, as a consequence also the threshold frequency and the dispersion relation change moving through the width of the waveguide. In particular, at the edges the internal field is reduced, hence also the threshold frequency for exciting the spin waves is lower. This means that a range of frequency exists for which only edge spin waves are excited. In order to simplify the mathematical description an average of the static internal field is taken into account, which corresponds more or less to that one of the centre of the waveguide.

If the dipole-exchange regime is taken into account, one can observe that DE waves are more convenient than BVW ones, because they have an higher group velocity and then a better excitation efficiency [18, 19]. But there is also a very bad issue: when scaling is performed on the structure, the demagnetization field becomes more and more important because the edge region prevail on the centre region. In this condition, a very high external field is necessary in order to obtain pure DE waves.

### 2.4.5 Main Propagation Parameters

Besides the dispersion relations it is necessary to know the most important propagation parameters of the spin waves. The first one which will be discussed is the mean free path [20]:

$$\delta = v_g(f, n) \times \tau(f, n) \quad (2.49)$$

In the above expression  $v_g$  is the group velocity, instead  $\tau$  is the mean lifetime of magnon. They are both dependent on frequency and the mode number. The group velocity as usually is defined as:

$$v_g = \frac{d\omega(k)}{dk} \quad (2.50)$$

It represents the speed at which the waves propagate their energy or the information. Since one of the main goal for logic operations is to have high performance in terms of computing speed, the group velocity is a very important characteristic because it define the quality of the device. Another parameter that define the performance of a logic gate is the magnon lifetime, because it describes the capacity of spin waves to propagate before being attenuated. The attenuation is due to the damping phenomenon, hence it is necessary to allow imaginary part of the dispersion relations, indeed in this way it is possible to define the decaying behaviour [27]:

$$e^{i\omega t} = e^{i(\omega_r + i\omega_i)t} = e^{\omega_i t} e^{-i\omega_r t} = e^{-\frac{t}{\tau}} e^{-i\omega_r t} \quad (2.51)$$

As defined in the equation 2.51,  $\tau = -\frac{1}{\omega_i}$ . The analytical formula for the lifetime is suggested by [20]:

$$\tau = 2\pi \left( \alpha \omega \frac{\partial \omega}{\partial \omega_H} \right)^{-1} \quad (2.52)$$

where  $\alpha$  is the constant describing the damping effect, and  $\omega$  is given by the equation 2.44.

Taking into account what has been said before about the attenuation, the last parameter has to be defined:

$$I(x) = I_0 e^{-\frac{x}{\delta}} \quad (2.53)$$

According to the equation 2.53, in the region where spin waves are excited the intensity is equal to  $I_0$ , hence it is the initial intensity, then a decaying behaviour occurs in the x direction (propagation direction) as it is described by the exponential, which is influenced by the magnon mean free path  $\delta$ .

# Chapter 3

## Simulation Setting and Procedures

Since the work carried on in this thesis is based on the modeling of the device, it is necessary to set first of all the parameter of the computation and implementation, otherwise bad results can occur if the initial conditions are not correctly defined. Different aspects of the modeling work will be discussed in the following.

### 3.1 Waveguide Definition

The waveguide is the structure where the spin waves propagation takes place. As it has been said before, the geometry and the dimensions of the system strongly influence the modes propagating in it. Hence extremely attention has to be used in the choice of the waveguide.

Regarding the choice of the *material*, the types that can be used are permalloy and the compound  $Co_xFe_yB_z$ . They provide a low damping profile, this means that the spin waves can propagate in a good way. Since one of the excitation mechanisms used in IMEC is the magnetoelastic one,  $Co_{40}Fe_{40}B_{20}$  is preferred because the permalloy have zero magnetoelastic coupling. In order to set the desired material in the simulation, it is necessary to assign the proper values to the quantities that should characterize the material: the saturation magnetization is  $M_s = 1.25 \times 10^3 kAm^{-1}$  [21], then the exchange stiffness constant is  $A_{ex} = 1.89 \times 10^{-11} Jm^{-1}$  [22]. The

damping constant of this material is found to be  $\alpha = 0.004$ .

In order to choose the *geometry* several criteria have to be taken into account. First of all it is necessary to define the coordinate system exploited in this work:  $\hat{x}$  is the propagation direction and corresponds with the length dimension,  $\hat{y}$  is the width direction, instead  $\hat{z}$  is the thickness direction. The length of the waveguide has to be  $L > \lambda$ , in order to describe the propagation of the spin waves, otherwise it is impossible to have a clear idea about the spin waves properties in the waveguide. The second criterion is that if length increases it is possible to have more resolution in the spectral decomposition, when Fourier Transform is performed in space in order to find the wavenumber components. The last thing to be taken into account in the choice of the length is the number of inputs that one wants to include in the majority gate. In the case studied in this work three inputs are included. Hence the optimal value for the length is  $10 \mu m$ : indeed if the length is higher it is possible to include a larger number of inputs, but the computational time increases strongly. Since the goal of the thesis is to study the dynamic behaviour of the majority gate three inputs are sufficient. Regarding the number of inputs it is necessary to take into account the size of the cell and the distance between one cell and the next one. In this case the cell is  $300 \text{ nm} \times 800 \text{ nm} \times 30 \text{ nm}$ , and the distance between two consecutive inputs has to be an even or odd multiple of the wavelength (this aspect will be discussed in detail in the chapter 5). Furthermore one has to consider also the space necessary at the boundary of the structure for the damping profile. A trade off is made through the parameters described.

The width has to be small enough to satisfied the scaling requirements, but it cannot be too small because of the shape anisotropy which increases when the structure size decreases, due to the demagnetization field. Finally the thickness has to be small enough to allow the approximation of the zero order thickness mode, according to which the spin waves profile is constant across the thickness.

At this point one can states that in the analyzed structure there are several regions: the excitation area, the propagation area and the damping area (see figure 3.1).

Finally the damping profile has to be discussed. Supposing that the origin of the coordinate system is in the middle of the waveguide, one can states that between  $-3.9 \mu m$  and  $3.9 \mu m$  the damping has the lowest value, which corresponds to the typical value of the CoFeB ( $\alpha = 0.004$ ). But it is not

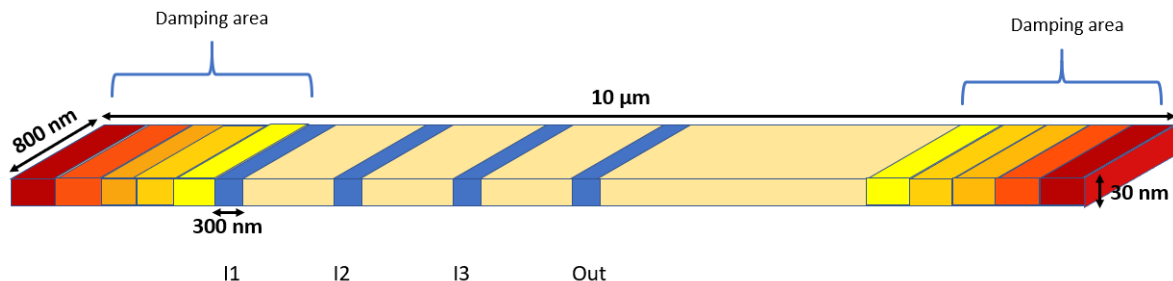


Figure 3.1: The structure is divided in different areas: going towards the edge the damping value increases, in order to kill the reflections, in the region in the range  $[-3 \mu\text{m}, 3\mu\text{m}]$  (taking into account that the origin of the reference system is in the centre of the waveguide), the value of the damping is the lowest one. The reason why is because here the propagation of the spin waves has to take place.

constant for the entire length of the structure. At the edge the damping has to be higher than in the middle, because spin waves are reflected at the boundaries of the structure, hence in order to avoid the back scattering spin waves have to be attenuated before reaching the edge. But at the same time, if the damping is too high and its profile is too sharp, the back scattering occurs, because it is not possible to attenuate the spin waves in a fast way so they continue their propagation after inverting the direction. Ideally the damping profile can be described analytically as follows [23]:

$$\alpha = \alpha_0 + \frac{\Delta\alpha}{2} \left[ 1 + \tanh \left( \frac{|x| - R_0}{\Delta R} \right) \right] \quad (3.1)$$

Here  $\alpha_0 = 0.004$ ,  $\Delta\alpha = 1$ ,  $R_0 = 4.9\mu\text{m}$ ,  $\Delta R = 150\text{nm}$  and  $x$  is the propagation direction in the range  $-5 \mu\text{m}$  and  $5 \mu\text{m}$ . The equation 3.1 represents a smooth increase of the damping toward the edge of the waveguide. Since in the software Mumax3 it is not possible to implement this equation, the method exploited is to divide the damping region in very small areas, and assigning to each of them a value for the damping obtained by the analytical curve. Furthermore it is not so easy to obtain a certain damping profile in the experiment. Indeed if one wants to implement different values of damping, different materials have to be exploited. Hence there are two main issues: it

is difficult to find a material with a specific damping value, as it is required according to the equation 3.1, then also the fabrication process becomes more complex, because the waveguide involves several materials. The alternative solution is to make the waveguide longer, and this last one is the trick used in laboratory, because it is the easiest one. Indeed if the waveguide is built in a way that when the spin waves reached the edges are already attenuated, the reflections will be very weak, or in the best case they are absent. The additional length needed to obtain this effect has to be higher than the mean free path of magnons: in this way one can be sure that the spin waves are died before reaching the edges. Hence in the experiment the utilized structure is bigger than that one used in the simulations. In this last case is better to exploit the method of the damping profile, because make a longer structure implies more computational time.

## 3.2 Software for Micromagnetic Simulations

*MuMax*<sup>3</sup> is an open source program for micromagnetic simulations. It computes the space and time dependent magnetization dynamics in nano- to micro-sized ferromagnets using a finite-difference discretization [24]. According to the working principle of the software, every cell is represented as a macrospin. Since the differential equation is discretized in time, at each time step  $H_{eff}$  is computed in every space step, and then the value obtained is exploited for the resolution of LLG equation with a numerical method: Runge-Kutta is the method used in this thesis. Regarding the size of the cell chosen for the space discretization, some notes are necessary: the dimension of the cell needs to be the same order or smaller than the exchange length, because this is the shortest range interaction. Furthermore the size has to be smaller than the wavelength, otherwise bad results are obtained since it is not possible to see the real propagation of the waves. From these factors, it seems that it is better to decrease the cell size, but it has an high cost in terms of time computation. Hence a trade off is made and finally the cell size is defined as  $5 \times 5 \times 10 \text{ nm}^3$ .

### 3.3 Ground State Computation

One of the most important setting, before starting a simulation is the ground state. It corresponds to the minimal energy state, hence it is the equilibrium state. If no dynamic excitation is applied to the system, after a certain relaxation time equilibrium is reached, and in the figure 3.2 the resulting magnetization components are shown. As it is clear the magnetization should be constant along the  $\hat{y}$  direction, but near the edges it is subjected to a sharp change, because of the presence of the demagnetization field.

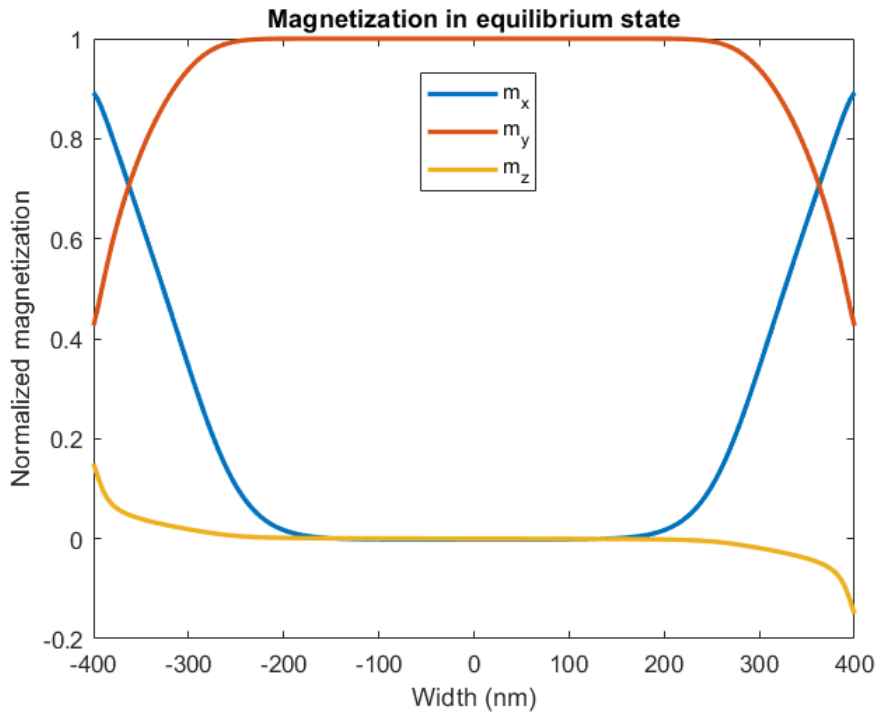


Figure 3.2: The ground state magnetization is normalized respect to the saturation magnetization  $M_s$ , and it plotted as a function of the width, in order to show the effects of the shape anisotropy.

In order to obtain this state first the spins have a random orientation, then an external static field is applied  $H_{ext} = 100mT$  in the  $\hat{y}$  direction: the system after a while will reach the ground state (figure 3.3). The direction chosen

for the static field, aims to obtain a DE geometry, indeed the magnetization of the material will be perpendicular to the dynamic field, applied in the  $\hat{x}$  direction. The criteria that can be used to stop the simulation when ground state is achieved are several: MuMax3 has implemented in the program the relaxation function, according to which the system is brought as closely as possible in the minimum energy state. But it is difficult to be sure that the reached state is not only a local minimum. For this reason a better criterion is exploited: the evolution is run until  $\left| \frac{dm}{dt} \right| > 0.01 \frac{\text{degree}}{\text{ns}}$ . As already said in the previous section, demagnetization field gives rise to the shape anisotropy, hence at the edge of the structure the magnetization is not well aligned with the external applied field. In the computation of the ground state this non homogeneity is present, and this means that it will influence every evolution of the system because the ground state is the starting condition. In the real world it is impossible to avoid the shape anisotropy issue, but in the simulation one can exploits some tricks, in order to obtain a uniform magnetized waveguide. This uniform ground state (3.4) is used in the computation of the lifetime, in order to have a more feasible value for the DE waves. The idea to obtain the uniform ground state is to apply a compensating field, in addition to the external one, in order to cancel the demagnetization field. Firstly it is necessary to know the profile of the demagnetization field, which is not constant, and in particular it has higher value near the edge, hence this means that the internal field decreases as it approaches to the edge of the structure. If the initial magnetization is initially set oriented in the  $\hat{y}$  direction, and then the system is left free to evolve for a small interval of time, in the order of femto seconds, MuMax3 is able to compute the demagnetization field. Indeed the established initial magnetization is the ideal one, and the system cannot stay in that state, because it is not the minimal energy state, hence the demagnetization has the power to bring the system in the equilibrium. Once this value is known, it is possible to run a new simulation for the computation of the ground state. In this case the internal field is given by [4]:

$$H_{eff} = H_{ext} + H_{demag} + H_{comp} = H_{ext} + H_{demag} + (-H_{demag}) = H_{ext} \quad (3.2)$$

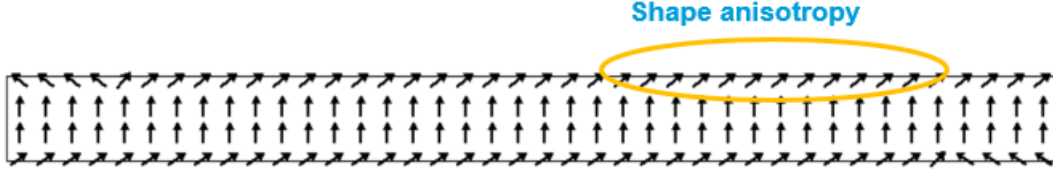


Figure 3.3: The spins are oriented perpendicularly to the propagation direction (DE configuration), but at the edge shape anisotropy is present.

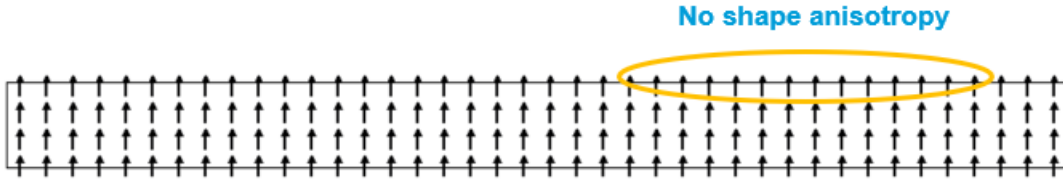


Figure 3.4: The compensation of demagnetization field allows to obtain a uniform ground state, without the shape anisotropy.

If this method is exploited the internal field will be exactly equal to the applied external field. In the figure 3.5 the profile of the demagnetization field is shown.

### 3.4 External Excitation

The magnetization of the material, hence the excitation of spin waves is externally controlled. There are different ways to excite the waves in the device, such as the magnetoelastic excitation, which is realized through the magnetoelectric cells. In the case studied in this work, antenna excitation is employed. It can be thought as a circular wire placed on the top of the waveguide, with a uniform distribution current inside. The field yielded by the wire is equal to:

$$H_{antenna} = \frac{I}{2\pi(R+r)} \quad (3.3)$$

where  $I$  is equal to the current inside the wire,  $R$  is the radius of the wire, and  $r$  is the distance from the antenna. Even if the field should depend on the

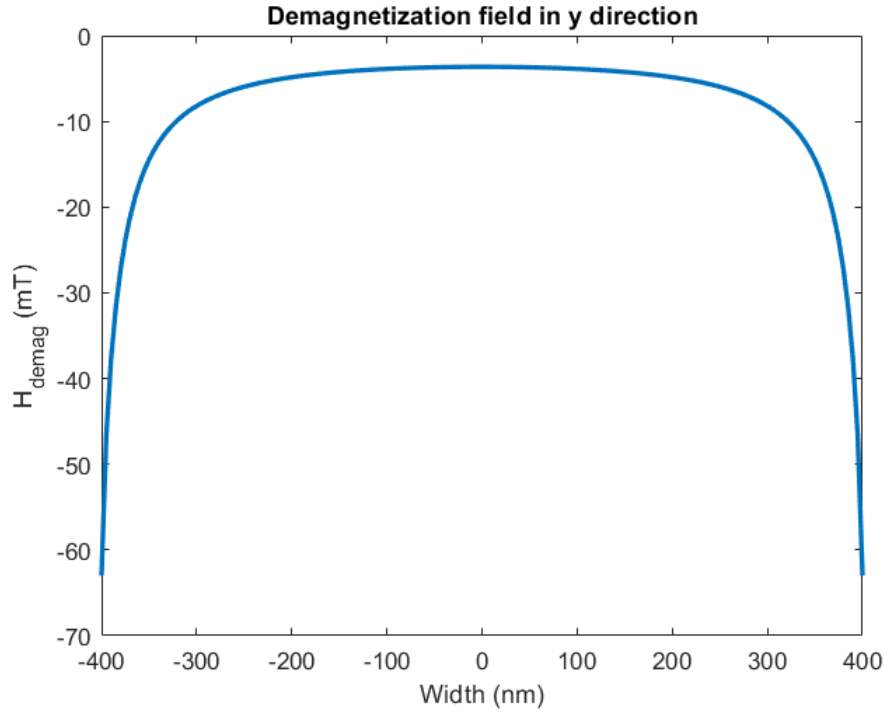


Figure 3.5: The demagnetization field is plotted as a function of the width. The software Mumax3 put the origin of the coordinate system in the centre of the waveguide, hence the x axis has the range [-400 nm, 400 nm].

distance from the excitation region, in a small waveguide the field is considered uniform in the waveguide. The direction of the field can be established changing the orientation of the antenna.

# Chapter 4

## Spin Waves Characterization in the Majority Gate

In this section the main characteristics of the spin wave propagation are analyzed and the difference between the analytic and numerical method is showed. Indeed the analytic results are very idealistic, but the numerical ones are more realistic and they give a clear idea on the working of the spin wave devices, underlying all the issues that prevent this new technology to replace the CMOS one.

In the section 4.1 dispersion relations are shown in different cases, then in section 4.2 lifetime computation method is explained and in the end in section 4.3 group velocity is obtained.

Regarding the lifetime and the group velocity only the Damon-Eschbach ( $M \parallel \hat{y} \perp k$ ) configuration results are shown, because BVW ( $M \parallel \hat{x} \parallel k$ ) case are negligible for the purpose of this dissertation, even if in the section of dispersion relations BVW analytic case is shown in order to compare it to the configuration used in the device.

### 4.1 Dispersion Relations

The dispersion relation  $\omega(k)$  describes the relation between the frequency and the wave number, hence the oscillation in time and space. Computing the dispersion relations is a crucial point because it allows to see which modes are excited in the guide, for a certain configuration (DE or BVW).

In order to perform this computation, the following approach is used: a uniform pulse of 20 ps is applied in the guide with an amplitude equal to 1 mT. This pulse in time corresponds to a sinc function in frequency space with the first node at  $f=50$  GHz; this means that all frequencies below 50 GHz are excited. The pulse is applied in a region equal to 300 nm in  $x$  direction, 800 nm in the  $y$  direction and 30 nm in the  $z$  direction. Moreover the antenna is placed, in the  $x$  direction, at  $x = 2\mu m$ . The goal is to obtain the frequency as a function of the wave number, hence a Discrete Fourier Transform is computed using the following formula:

$$M[f, k] = \frac{1}{\sqrt{XT}} \sum_{x=0}^{X-1} \sum_{t=0}^{T-1} m_z[t, x] e^{-i2\pi(\frac{tf}{T} + \frac{xk}{X})} \quad (4.1)$$

In the formula  $m_z[t, x]$  is the dynamic out of plane component of the magnetization in time  $t$  e position  $x$ ,  $X$  is the total length of the sample ( $10\mu m$ ),  $T$  is the total simulated time (10 ns) and  $M[f,k]$  is the result of DFT for the frequency  $f$  and wave number  $k$ .

Some precautions must be taken into account in the interpretation of the results. The change in magnetization should be larger than the cell size in order to obtain realistic results, hence the magnetization has to be uniform in every cell because in that way the cell is considered as a macro spin. For this reason the maximum wave number is  $100 \text{ rad}/\mu m$  (the wavelength in this case corresponds to 63 nm), since the cell size is 5 nm and then the wavelength is more than ten times larger than the cell.

In the figure 4.1 it is possible to compare the numerical curve with the curves obtained by the equations in the chapter 2. The two dotted line are fitted quite well by the analytic curve that describe the DE mode 1 and the DE mode 37. Instead regarding the BVW analytic dispersion relation, it is supposed to have a zero field along  $x$  direction (because in order to have a DE configuration the external field is applied only in  $y$  direction) and then it is supposed to have  $n=3$  for the mode number, since it is the first mode for BVW wave that can exist at  $f=13.82$  GHz. Furthermore from the plot it can be deduced the wavelength corresponding to the operating frequency of DE mode1 at which the device is simulated (13.82 GHz): it is equal to  $\sim 1 \mu m$ . The analytic computation of the dispersion relations requires some precautions, in order to be well fitting with the numerical curves. The influence of the non-uniform magnetization on the spin wave behaviour must be taken

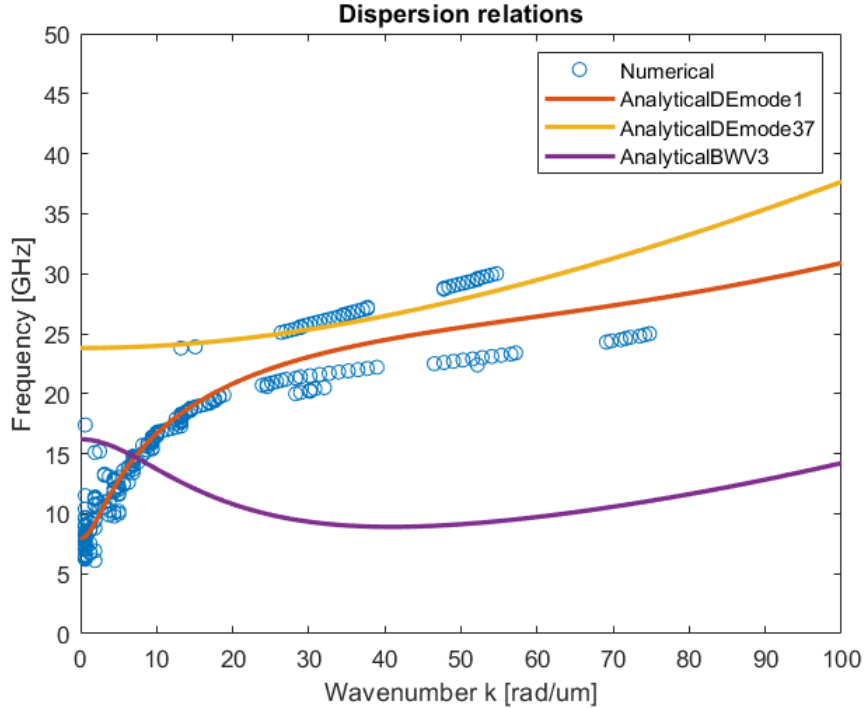


Figure 4.1: Dispersion relations of the device: in the plot different curves are present. The numerical curve (dotted line) is obtained from the simulation, the analytic curves instead are obtained from the equation shown in chapter 2.

into account, as it is explained in chapter 3, hence the external field should be the same as that one computed by mumax3. This means that, even if a magnetic field equal to 100 mT is externally applied, the effective field received by the waveguide is smaller.

In the plot of dispersion relations it is also possible to detect the FMR frequency (8 GHz), since it corresponds to  $k=0$  rad/ $\mu\text{m}$ : the FMR frequency can be considered as the frequency where all the spin precess with the same phase, hence the wavelength could be infinite. For  $k > 30$  rad/ $\mu\text{m}$ , the analytic curve for mode 1 seems to move away from the numerical one: this could be justified by the fact that the analytic dispersion relations are obtained with some approximations and, mainly, in the waveguide there are BVW waves, excited by the field at the edge of the sample. This means that the numeri-

cal dispersion relation is not perfectly correspondent to a DE configuration, but it shows an intermediate behaviour between DE and BVW waves. This hypothesis is demonstrated by the simulation performed in the next chapters.

## 4.2 Lifetime Computation

The lifetime describes the decay of the amplitude of the wave in time, as it is explained in the chapter 2. In this section the numerical method to obtain lifetime is described and then it is compared to that one derived by the analytic formula, exploiting the dispersion relations.

Before getting the desired result, some assumptions are required. As it has been done for analytic dispersion relations, also in this case it is necessary to take into account the magnetization non uniformity in the waveguide, in order to obtain a lifetime not influenced by the distortion due to the geometry of the device. Hence in the following paragraph the adopted method is explained.

First of all an external field is applied in order to align the spin along the  $y$  direction. In this external field, the demagnetization field is taken into account, so the effective field applied to the system is subjected to a compensation, as explained in the chapter 3. Then an exciting sinusoidal field (amplitude equal to 3 mT and frequency equal to 13.82 GHz) is applied up to 3 ns, in order to allow the system to reach the steady state; after this time interval the field is stopped and without an excitation the system releases, hence the amplitude of magnetization gradually decreases. If Fourier Transform is performed in space at different time intervals, it is possible to see all the components in frequency present in the sample at a specific time and their respective amplitude. This means that it is possible to follow the decay in the amplitude of the frequency at which the device operates.

Computing the DFT in space for each considered time interval and taking the value of the spectrum that correspond to the operating wave number of the device, it is possible to see the decay in the magnitude of that component. The extrapolated data are interpolated and an exponential fit is exploited: in this case the plot (figure 4.2) can be approximated with the equation 4.2 where  $\tau$  is the lifetime and it is  $\sim 3$  ns.

Numerically only the lifetime of one component is obtained, because computing the lifetime as a function of the wave number requires a big effort

and it is not necessary in this dissertation because it is supposed that the device has to work with only one frequency. But analytically it is possible to obtain the plot of lifetime with regard to the wavenumber and it is shown in figure 4.3. In the analytic case the lifetime corresponding to the wave number  $k=6.29 \text{ rad}/\mu\text{m}$  is equal to  $\sim 5 \text{ ns}$ . This value seems a little bit different from that one extrapolated by numeric method, but this is due to different approximations, for example that one done on the damping profile: indeed in the analytic case the damping is considered as a constant, instead in the simulation the damping has a certain profile, this means that it changes in the wave guide, as explained in chapter 3.

$$f(t) = f_0 \exp\left(-\frac{1}{\tau}t\right) \quad (4.2)$$

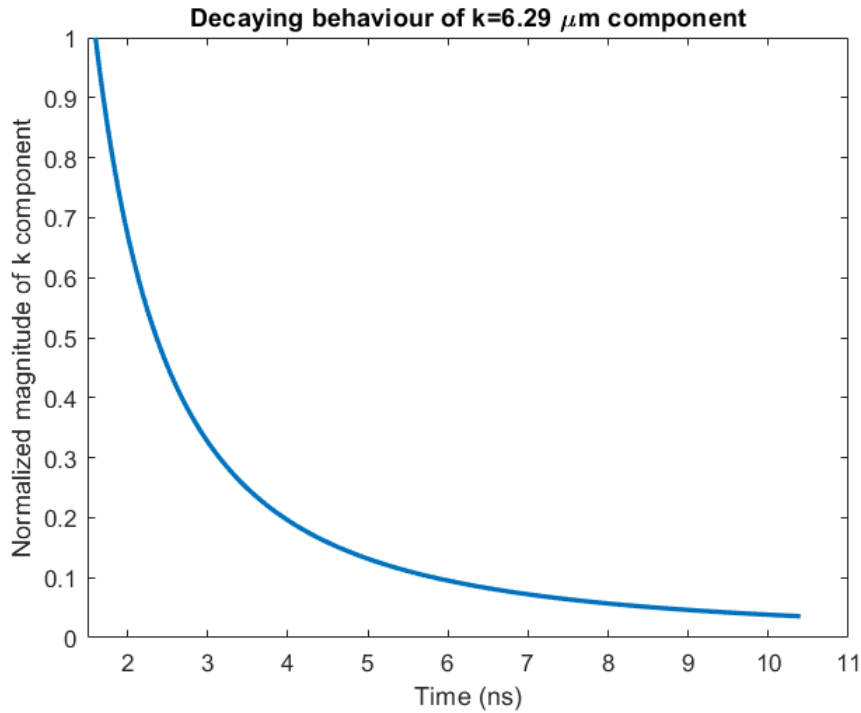


Figure 4.2: This plot represents the decay in time of the Fourier Transform of the  $k$  component equal to  $6.29 \text{ rad}/\mu\text{m}$ .

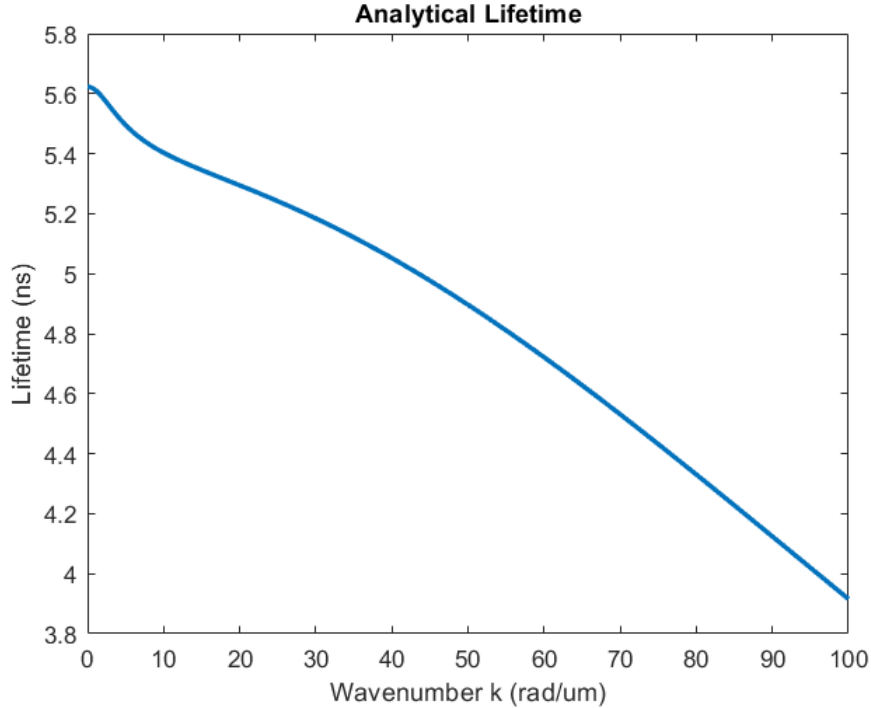


Figure 4.3: Analytic lifetime is plotted for DE configuration mode 1; the external field considered is that one obtained from the compensation of the demagnetization field.

### 4.3 Group Velocity Computation

The group velocity describes the magnons speed traveling through the waveguide and, as explained in the chapter 2, this propagation characteristics corresponds to the derivative of the dispersion relation with respect to the wavenumber. Considering the numerical dispersion relations and taking into account only the branch related to the mode number 1 of DE configuration, it is possible to interpolate these points in order to obtain a well fitting curve. Then derivative is computed on this curve and the group velocity plot is obtained by numerical method. Instead for the analytic curve of the group velocity the derivative is computed on the dispersion relations obtained by the equation 2.44. In the figure 4.4 it is possible to see the comparison between the analytic and numerical curves. The range taken into account goes from  $3 \text{ rad}/\mu\text{m}$  to  $100 \text{ rad}/\mu\text{m}$ : the upper limit is due to the fact that the

wavelength of the magnon wave has to be larger than the cell size of the simulated mesh, for this reason it is better to not consider  $k$  value higher than  $100 \text{ rad}/\mu\text{m}$ ; instead regarding the lower limit it is chosen in order to avoid the issues related to the numerical curves fitting approximations, that can cause a misleading in the interpretation of the results. The group velocity value is a little bit different in the two cases, but as already explained regarding the other discussed propagation parameter, this is due to the sum of all approximations made in the computation of the analytic curve, and it is also due to the fact that the numerical data are interpolated with a linear regression method, so other type of approximations occur. Hence in the end it is better to say that the group velocity has a value included between the analytic case and the numerical one. A better value will be obtained in the section 5.1, because in that case the group velocity, instead being computed from the numerical dispersion relation, it will be computed directly looking to the snapshot in sequence, obtained from the simulation of one input propagation in continuous regime.

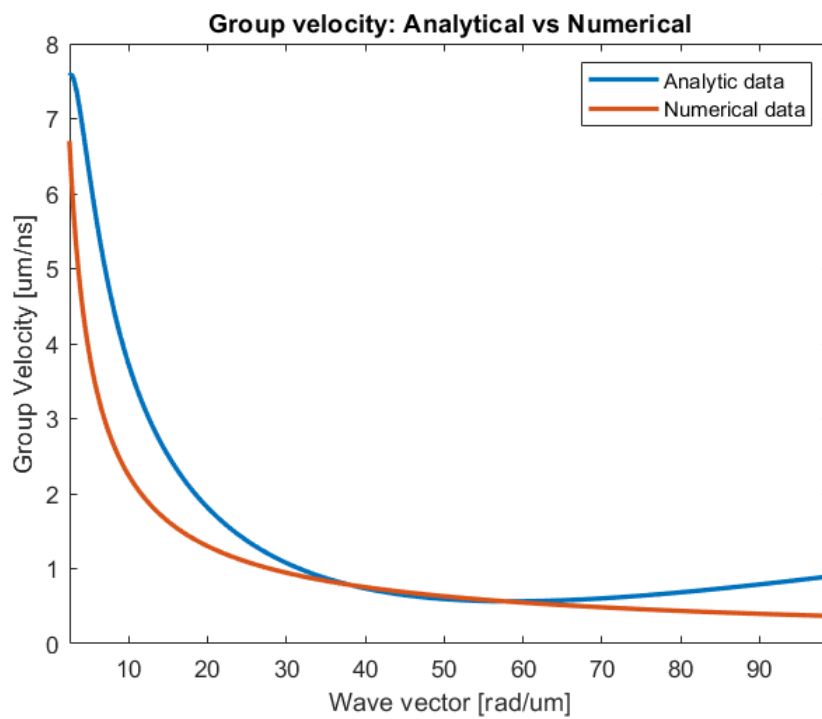


Figure 4.4: The group velocity corresponding to  $k=6.29 \mu\text{m}$  is equal to:  $3.23 \mu\text{m}/\text{ns}$  in the numerical case and  $5.33 \mu\text{m}/\text{ns}$  in the analytic case.

# Chapter 5

## Continuous Regime

In this chapter majority gate functions in continuous regime are analyzed. This is the most simple case but it is very useful to understand how the spin waves propagate in the magnetic sample. If spin wave are excited by a continuous signal only one frequency will be present in the guide, and it corresponds to the frequency of the signal applied. In this chapter of the dissertation a sinusoidal signal is exploited and the frequency is equal to 13.82 GHz, in order to deal with the experiments performed. Spin waves, in the ideal case, should replace the already existing electronic circuits, so the higher is the frequency the smaller is the wavelength, and this implies better device performance in terms of computation and scaling, but if the frequency overcomes a certain limit other modes can arise in the guide and there will be interference between them. In order to avoid the drawbacks, a trade off is required. In order to describe the functions of a majority gate it is necessary to apply some inputs (three in the case of this dissertation) and to analyze the output. When external field is applied in the magnetic sample the system will be subjected to several physics phenomena, hence the output is not perfect as someone could expect. In this section, first, one input propagation will be showed and analyzed (5.1), in order to see what happens in the most simple case and then the other two inputs will be applied for describing the interference pattern (5.2).

## 5.1 One Input Propagation Analysis

The propagation of one input is performed applying an oscillatory field corresponding to the following shape:  $s(t) = A \sin(2\pi ft)$ , where  $A$  is the amplitude and it is equal to 1 mT and  $f$  is the frequency and it is equal to 13.82 GHz. It is very important to carefully choose the amplitude of the excitation field, because if it is too small there is not enough energy to excite the spin wave, instead if it is too high the system is brought in a non linear regime, where the dynamic becomes complex and it is not possible to have the functions of a majority gate. Regarding the choice of the frequency, it is necessary to take into account the trade off between the power consumption and the scaling: indeed, as it is clear looking to the dispersion relation, if the wave number increases the frequency also becomes greater. Hence a smaller wavelength implies larger power consumption, because the spin waves requires a greater frequency to be excited. Then the value 13.82 GHz is the right compromise to have a good trade off because it allows to have a wavelength in the range of  $\mu m$ , hence a structure in the nanoscale. The antenna is placed at  $2 \mu m$  from the left edge of the sample and the damping is applied only along the x direction according to the profile described in the chapter 3. In the figure 5.1 it is clear that, starting from the ground state described in the chapter 3, when field is applied, the spin waves start to travel from the point where antenna is placed, and then they propagate as the simulation time flows.



Figure 5.1: The snapshot represents the component  $z$  of the magnetization and it is captured at  $t=0.2$  ns. In the figure it is possible to see two irregularities at the left upper corner and the right bottom one: they are artifacts of simulation due to the geometry of the sample, that has to obey to the well known anisotropy law of magnetism. In the chapter 3 this phenomenon is clearly showed in the snapshot of the ground state.

At the edge of the sample along the  $y$  direction, the ground state magnetization is not perfectly aligned along the  $y$  direction, but it is tilted on the  $x$  direction. If the initial magnetization and the applied excitation field are not perfectly perpendicular, there will be other type of waves in the wave guide, not only DE ones. Indeed, at the edge the angle between the oscillatory field and the magnetization is  $0 < \theta < 90$ , this means that it corresponds to an intermediate case between the BWV and DE configuration. Starting from the edge these intermediate waves propagate along the  $x$  and  $y$  direction, hence the interfere with the DE waves propagating in the middle of the waveguide. Despite this interference between DE waves and the intermediate ones, the spins keep the same phase between them, hence the spin wave keep going on in the waveguide, but change occurs in the pattern of them as it is described in the figures 5.2 and 5.3.



Figure 5.2: The snapshot is taken at 0.5 ns. The intermediate waves become more relevant as the time flows, but far from the antenna the pattern is still the same as that one of the begin.

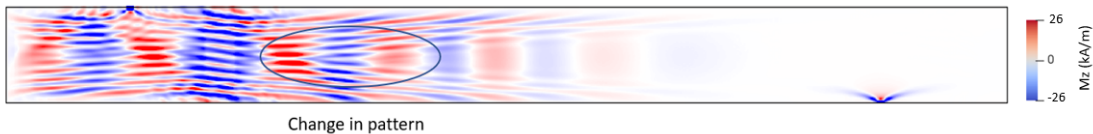


Figure 5.3: The snapshot is captured at 0.72 ns. It is clear that the pattern starts to change near the antenna, but as the time flows this change will propagate along all the waveguide if the simulation is long enough.

Furthermore the intermediate waves reach the middle of the width after 0.5 ns this means that their group velocity is equal to  $\sim 0.8\mu m/ns$ : considering the group velocity obtained for DE waves in the section 4.1, it is clear that intermediate waves are slower than DE ones.

The ideal condition would be that no intermediate waves propagate in the waveguide but only pure DE waves. Unfortunately this is impossible, due to the fact that the device is confined, hence it has necessarily geometry edges subjected to the effect of shape anisotropy (detailed description of this phenomenon is present in chapter 2 ). Despite this fact, it is possible to exploit some adjustments to attenuate the intermediate waves, even if they will be always present. The same trick used for the reflected waves in correspondence of edges along the x direction can be used in this case: this means that a damping profile can be set along y direction. In this way the intermediate waves will have a lower intensity (figure 5.4), even if the change in the propagation pattern occurs as it happens in the case where no damping is applied on y direction.



Figure 5.4: This snapshot is taken at 0.5 ns, hence in the same time of figure 5.2. In this case the red and blue line in  $x=2\mu m$ , where antenna is placed and where intermediate waves start to propagate, are still separated if you look along y direction, instead in the other figure, in the same position, the red and blue line alternate along y direction.

The only advantage that can be gained with this method is more separation between the two bit 0 and 1, that are represented respectively by a certain  $\phi$  and  $\phi + \pi$ , as already explained in the chapter 1. Despite the fact that the binary code is read by the phase, and hence by red and blue color, it is important to underline the fact that the phase is determined by the average color present in a certain position along x. This means that, even if in a x position there are red and blue lines alternated, the phase is established by the preponderant color. For this reason, in the worst case, where there is no damping on y direction, the phase in a specific position along x is still readable.

Realizing a damping profile is not so easy during fabrication process, as it is explained in chapter 3, and also make the width larger is not a feasible solution, because of the scaling, hence from here on out all the cases discussed are referred to the situation in which no damping profile on y direction is applied.

In order to read the correct result, the output window must be placed at a distance  $d=n \lambda$ , where  $n$  is a positive and natural number,  $\lambda$  is the wavelength of the spin waves. In this way the same input will be read in the output, because they are in phase. Instead if the inverter function has to be realized, the output has to be placed in the position indicated by the equation 5.1, because in this way the input and the output are out of phase, with a shift equal to  $\pi$ . In the figure 5.5 this concept is clearly showed. In continuous regime the wavelength is more or less the same along all the length of the device, if intermediate waves influence is considered negligible, differently from the pulsed regime where a broadening of the spectrum occurs (this will be discussed in the next chapter 6). Hence if the wavelength is more or less the same in every position, the output could be placed in any point, respecting the rule about the distance  $d= n\lambda$ . Despite this advantage it is better to place the output as close as possible to the input in order to reduce the interval time necessary before reading the output, because the spin waves have to reach the output during the propagation. The group velocity of spin waves, that in this case corresponds to the phase velocity because there is only one component, is equal to  $5\mu m/ns$ , indeed this value is in the range  $[3.23\mu m/ns, 5.33\mu m/ns]$ , as predicted in the section 4.3.

$$x = \frac{1}{2}(2n + 1)\lambda \quad (5.1)$$

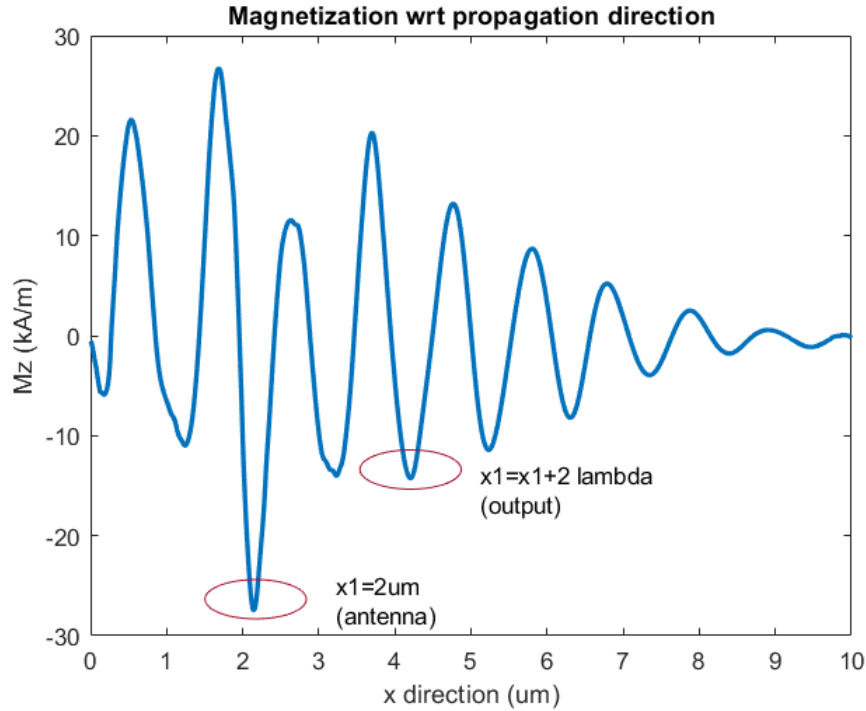


Figure 5.5: This plot represents the component  $z$  of the magnetization in the space (along the  $x$  direction) at a specific time (1.5 ns). It is clear that if the output is placed at a distance equal to a multiple of the wavelength the phase is equal to that of the input one. The output can be read only if the spin waves reached the output position, hence is very important the time at which the output has to be read.

## 5.2 Interference Pattern Analysis

The real working of the device is implemented with three or more inputs, because the logic function of this gate requires at least three inputs in order to apply the majority principle. Hence the first part, about one input only, is useful to understand the propagation of spin waves in the magnetic waveguide but it doesn't reflect the reality. In this section two other inputs will be applied in order to realize the logic function represented in the table 5.1. Including three inputs in the majority gate means that three antennas have

I1	I2	I3	OUT
0	0	0	0
0	0	1	0
0	1	0	0
0	1	1	1
1	0	0	0
1	0	1	1
1	1	0	1
1	1	1	1

Table 5.1: Taking into account  $n$  inputs, the value of the output is false if  $n/2$  or more arguments are false, and true otherwise.

to be placed in the magnetic sample at specific positions. The frequency used for the signals is the same used in the case of one input only. Hence three sinusoidal field will be applied along the  $x$  direction. It is supposed that in order to obtain an interference pattern, the spin waves generated by this three excitations have to propagate at the same time. The purpose can be reached following several approaches. First the most efficient method will be explained in detail, then the other methods will be described and compared to the first one.

### 5.2.1 Ideal Working Principle of Majority Gate

The designed device has a simple and rectangular shape, hence the three signals are placed successively in row, on a single line (figure 3.1). From this configuration the interference among the three inputs is necessary, because the spin wave generated by the first input will overlap with that ones generated by the second input, and finally they meet the waves of the third input, propagating along the length of the device. In this section it is supposed that the signals are applied in the same moment (later the issues related to this choice will be discussed), hence there are two options for placing the inputs: it is possible to put the antennas at the same distance changing the phase of the signal (which has to be only  $0$  or  $\pi$ ) in order to obtain the bit  $0$  or  $1$ , depending on the Boolean configuration that is desired, or alternatively it is possible to place the antennas in different position, but in this case the device has to be tuned in order to find for each input which phase allows to the input

to be 0 or 1 at the output. In the first case the antennas are at a distance equal to a multiple of the wavelength, because in this way the interference due to the position is always constructive, hence there is no influence by the position of the input. But the signal applied can be  $S = \sin(2\pi ft + \phi)$  or  $S = \sin(2\pi ft + \phi + \pi)$ . This means that if the signals have the same phase there will be a constructive interference, but if they are shifted by a quantity equal to  $\pi$  there will be a destructive interference.

The equivalent concept of that one explained so far is the following: all the signals are sent in the inputs with the same phase, it is supposed to be  $\phi = 0$ , but the distance between one input and the next one assumes different value depending on the bit combination desired at the input of the device. In particular if the distance from the output is equal to  $d = (n + \frac{1}{2})\lambda$  a shift of  $\pi$  respect to the initial phase occurs, instead if the distance from the output is equal to  $d = n\lambda$  there will be no phase shift, hence the phase at the output is equal to the initial one. In every inputs combination the output window has to be distant from the last input a quantity  $d = n\lambda$ , in order to be unbiased in the interference mechanism among the inputs. This idea would mean changing the distance of the inputs for each configuration of the inputs, but this is impossible to be realized in the real world because the antennas are fabricated on the device, hence after the fabrication process they are fixed. Anyway this idea can be simulated by the software and it is a very nice example about the working principle of the spin waves and their capability in realizing the majority gate function. In the table 5.2 are illustrated the setting of the simulations in order to obtain every configuration of the three inputs and in the figure 5.6 is showed the correct working of the concept explained so far.

Configuration	I1 → I2	I2 → I3	I3 → Out
0 0 0	$\lambda$	$\lambda$	$\lambda$
0 0 1	$\lambda$	$\frac{3\lambda}{2}$	$\lambda$
0 1 0	$\frac{3\lambda}{2}$	$\frac{3\lambda}{2}$	$\lambda$
0 1 1	$\frac{3\lambda}{2}$	$\lambda$	$\lambda$
1 0 0	$\frac{3\lambda}{2}$	$\lambda$	$\lambda$
1 0 1	$\frac{3\lambda}{2}$	$\frac{3\lambda}{2}$	$\lambda$
1 1 0	$\lambda$	$\frac{3\lambda}{2}$	$\lambda$
1 1 1	$\lambda$	$\lambda$	$\lambda$

Table 5.2: For each combination of the inputs the distance between an input and the next one is indicated.

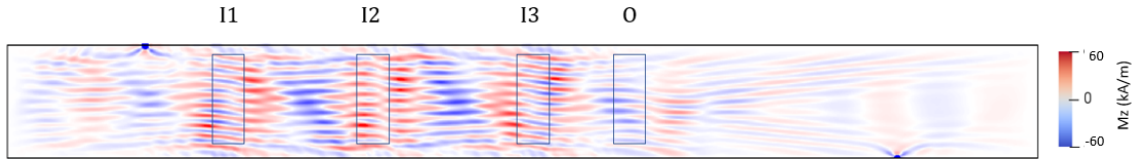


Figure 5.6: The figure shows a snapshot of the simulation and it represents the case 0 1 0 illustrated in the table 5.2. In this case the interval time before reading the output is greater than other case because the first and second inputs are farther from the output, so they took more time to reach the output window.

In the figure 5.7 it is possible to associate the red to the bit 0 (phase 0) and the blue to the bit 1 (phase  $\pi$ ), hence if the inputs are all 0, also the output is 0. Instead, as it happens in the figure 5.8, if the inputs have the configuration 0 1 0 (the configuration of the phase is 0  $\pi$  0) the output has to assume the value 0 because the majority of the inputs is equal to 0. The output window is placed at a distance  $d = \lambda$  from the last input: this is the minimum distance that allow to have a correct result. The time at which the output is read is also important, as it is said regarding the one input propagation, but in this

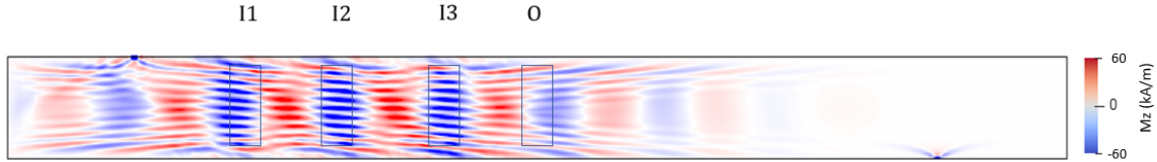


Figure 5.7: In the case represented in this figure the distance between the three inputs is  $n\lambda$  where  $n=1$ . The phase is  $\phi = 0$ : every signal has the same phase as the other inputs. Hence with these assumption also the output has the same phase of the inputs because there is a constructive interference among them. The snapshot is captured at  $t \sim 0.6$  ns.

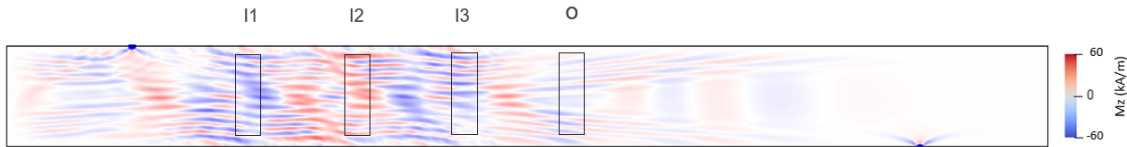


Figure 5.8: In the case represented in this figure the distance between the three inputs is  $n\lambda$  where  $n=1$ . The configuration of the inputs is equal to 1 1 0. The snapshot is captured at  $t \sim 0.6$  ns.

case the time is longer because there are three input. This means that the first input is the most far from the output, hence this is the limiting time: in order to read the interference among the three inputs, it is necessary that all three inputs reach the output and the first one takes the longest time (taking into account that the group velocity is equal to  $\sim 5\mu m/ns$  and the distance between the first input and the output is equal to  $3\mu m$ , the time is equal to  $\sim 0.6ns$ ).

Even if in the two figures the output is always zero, in the second case the spin waves look more attenuated than in the first case: this is due to the fact that when the inputs are in phase constructive interference occurs and this means that the amplitude of the waves increases because they sum each other. Instead when the inputs are out of phase destructive interference hap-

pens, then the amplitude decreases because they cancel each other. For this reason the bit zero (or bit 1, in other combinations) has not the same amplitude in all cases with the same result (figure 5.9), hence one can observe a strong majority, when the input combination has all the bits equal to each other, or weak majority, if only 2/3 inputs are equal, because in this case there is one destructive interference and one constructive. As a consequence threshold values has to be established in order to distinguish the phase of bit 1 and bit 0, otherwise this can cause a wrong interpretation of the results. The same logic works for all the other combinations of the inputs and this is clearly demonstrated by the simulation performed, but for sake of simplicity only significant examples are showed.

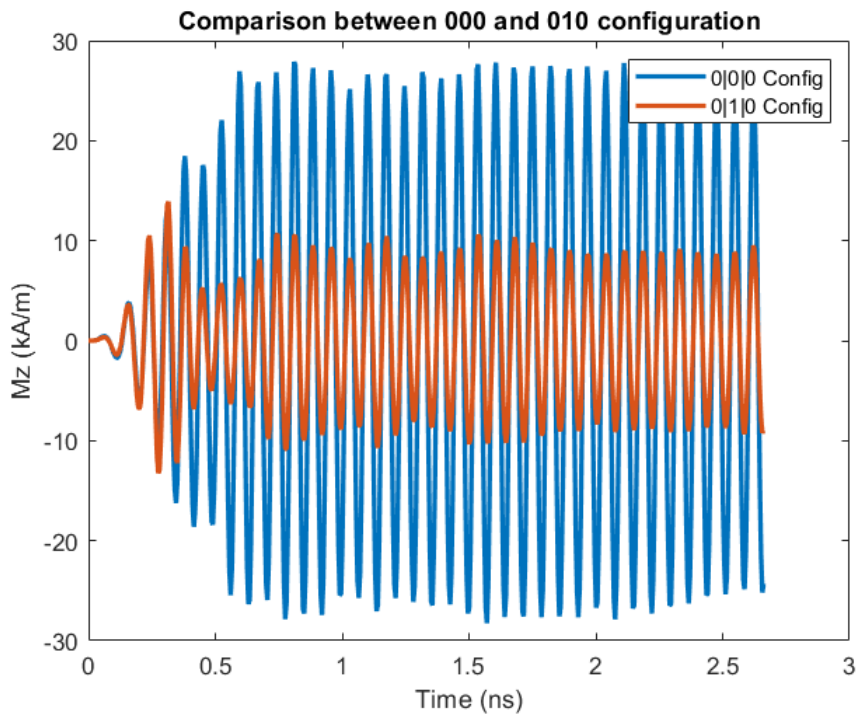


Figure 5.9: The figure shows the component  $z$  of the magnetization at the position  $x=5 \mu m$ , where it is supposed to have the output, respect to the time. The two plots corresponds to the two configurations described so far.

As it has been explained before there are different options to configure the

inputs, regarding the distance among them and their respective phase, in order to obtain a specific results. In the previous case the distance is kept constant among the inputs and the phase is 0 or  $\pi$  and it establishes the value of the bit. Hence now it will be described the case in which the distance among the inputs is not a multiple of the wavelength, but it assumes different values. First of all it is necessary to underline that the most feasible solution is that one in which antennas are kept always in the same position ( $d = n \lambda$ ), because in this case the physical implementation is easier, due to the fact that it can be handled using the same frequency for all signals and changing only the phase.

The main advantage of the method described now is that there are no restriction on the choice of the distance at which antennas are fabricated but in order to have the interference pattern that realize the majority gate it is necessary a great effort in order to find the signal parameter that allow to have the bit 0 or 1 at the output. Taking into account that the phase is  $\phi = \frac{2\pi x}{\lambda}$ , where  $x$  is the propagation distance and  $\lambda$  is the wavelength of the spin waves, knowing the distance that separate one input from the output it is possible to deduce the wavelength required in order to obtain the proper phase, and then a certain wavelength is obtained changing the frequency of the signal. Moreover if the phase for one bit is determined, consequently also the phase for the complementary bit is found because it needs only to be shifted of a  $\pi$  quantity. Despite this method looks very flexible, it is not efficient from the design point of view because for each inputs it is required a different frequency, depending on the distance from the output. For this reason nowadays only the first method is used.

The spin waves excited at the input position from the antenna take different time intervals to reach the output depending on the distance between the input considered and the output. Hence if the three inputs are sent in the same moment, when they reach the output they have different amplitude for the following reason: in the device different mechanisms occur such as scattering among spin waves, scattering due to phonons, and this phenomena are responsible for the thermal bath, which is the cause of the attenuation of spin waves during propagation. This loss in energy is described by the damping parameter (more details about the damping are found in the chapter 3). As a consequence the farther the input is placed the more attenuated it is when it will have reached the output. According to the figure 3.1, I1 is the most attenuated one at the output, instead I3 is the strongest one, because of the distance from the output window.

This phenomenon is not convenient, because of mismatching when they interfere. In order to avoid that, the signal at the input are scaled by a certain factor 5.2 in order to have more or less the same amplitude when they reach the output. In order to obtain the correct scaling factor, three different simulation have been performed. In each simulation only one input is applied but in different position, keeping constant the point of the output. In this way it is possible to see which is the amplitude, at the output, of the spin waves generated by the singular signal.

$$\begin{aligned} I1 &= k1 \sin(2\pi ft) & k1 &= 1 \\ I2 &= k2 \sin(2\pi ft) & k2 &= 0.7 \\ I3 &= k3 \sin(2\pi ft) & k3 &= 0.4 \end{aligned} \tag{5.2}$$

This matching depends only on the distance from the output, hence it can be exploited if the distance among the inputs is constant. Instead if the inter distance has to change in order to obtain the interference pattern, also the scaling factor has to change every time that a new configuration is sent in the majority gate.

### 5.2.2 Real Implementation of SWMG

In the simulations it is possible to establish a priori the phase of the inputs but experimentally there are some issues: it is not possible to know the phase at the inputs of the device, because the signal is brought to the antenna with a wire, and the phase depends on physical factors, such as the length of the wire, that induces some changes in the initial phase. The only way to perform a majority gate in experimental sense is to measure the phase shift at the output for each input and then from this result the input phase is obtained just tuning the signal up to the required phase. It is required that the phase of the individual SWs are matched at the output port where the waves interfere and furthermore, the microwave signals should be identical for a given logic level on all input ports: this is obtained by the resonant condition. This resonance is realized when the inter-port distance is  $N \times \lambda$ , where  $N$  is an integer number and  $\lambda$  is the wavelength of SWs.

As it has been said before, the bit 0 and the bit 1 have an amplitude or a phase that depends on the configuration that gives a certain result. This is due to the amount of the total number of constructive or destructive interference

that occur at the output position. In the experimental work that was realized to implement the majority gate in continuous regime, it is clear that all inputs configurations give different scattered power, measured through the scattering parameter technique (figure 5.10): even if each configuration has its own power, there is a common threshold that allow to separate the phase 0 (bit 0) from the phase  $\pi$  (bit 1) [25].

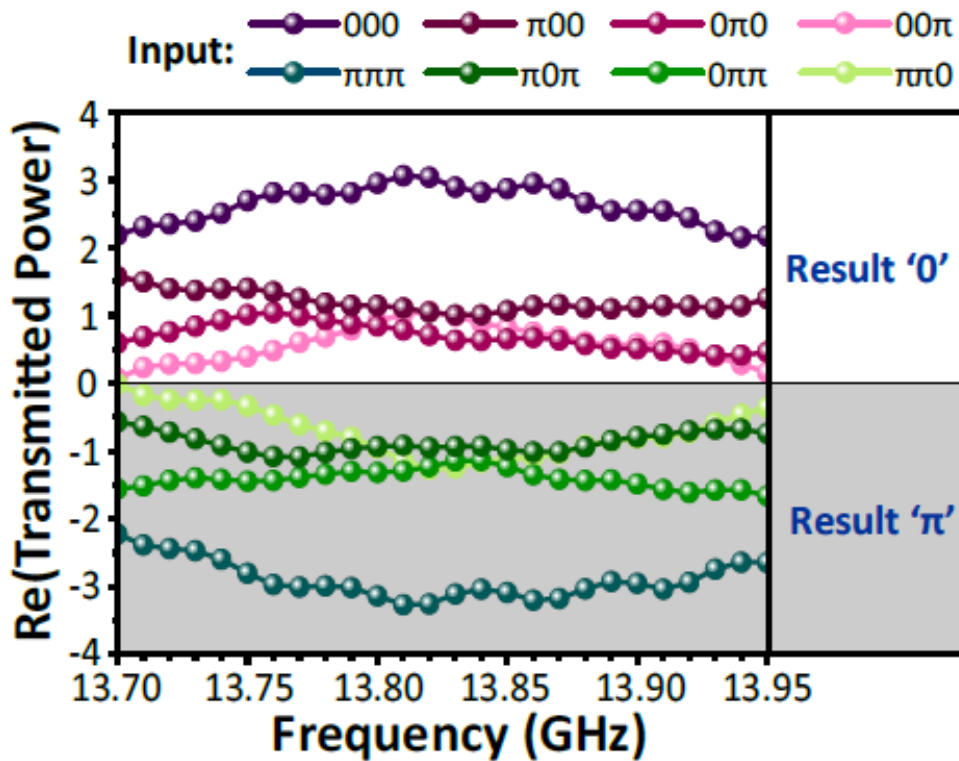


Figure 5.10: The plots is obtained in function of the signal frequency used to excite the spin waves in the system.

# Chapter 6

## Pulse Regime

So far the simplest behaviour of spin waves has been described, but the continuous regime is not sufficient for the electronics world, because thinking about the current CMOS circuit, the pulse regime is unavoidable to obtain higher and higher speed in the devices. This means that a circuit has to be able to change rapidly his output in order to increase the throughput and then consequently the computational power. As already said before in the chapter 1, the spintronic devices has the big advantage of much lower power consumption respect to the standard CMOS application. For this reason they could be a good alternative to the current electronics, but they need to have also the same performance in terms of speed and computational power. In this chapter the pulse regime, the most useful one, will be investigated and described in detail with the relative issues. In particular in the section 6.1 the Gaussian pulse with a carrying frequency is analyzed, instead in the section 6.2 rectangular pulse is described and then the two cases will be compared. Finally in the section 6.1.4 the repetition rate is discussed in order to understand if the device is able to perform consecutive operations and which is the recovery time between them.

### 6.1 Gaussian Modulated Pulse with Carrying Frequency

In this section the signal taken into account is a modulated oscillatory field by a Gaussian shape (figure 6.1). In particular the carrying signal has a

frequency  $f=13.82$  GHz, the same used in the continuous regime case, the amplitude instead is about 3mT. In pulse regime the amplitude has to be greater because the excitation is applied for short time and it has to be enough strong to generate spin waves able to propagate up to the output. Even if the amplitude in this case is higher, it needs to keep below an upper limit because otherwise non linear effect can occur, and this is a big issue since the behaviour of spin waves becomes rather complex, hence the dynamics cannot be understandable. The modulating signal instead is that one described by the equation 6.1, where  $A$  is the height of the peak,  $\mu$  is the position of the center of the peak, also called average of the pulse, and  $\sigma$  controls the width of the shape and it is called standard deviation of the Gaussian function.

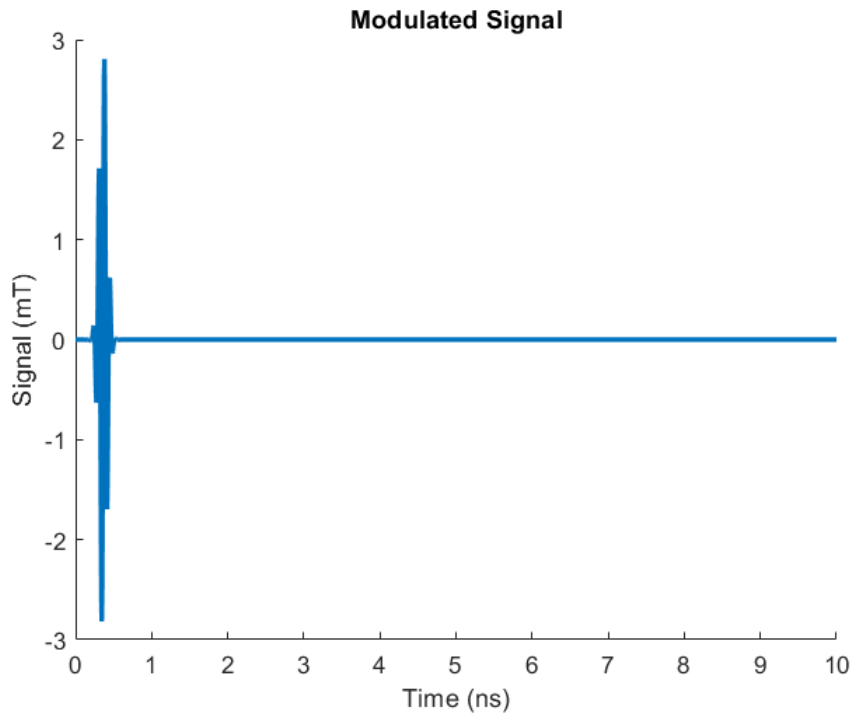


Figure 6.1: This is the modulated signal composed by the sinusoidal (carrying) and Gaussian (modulating) ones.

$$\begin{aligned}f(t) &= A \exp\left(-\frac{(t - \mu)^2}{2\sigma^2}\right) \\A &= 3mT \\ \sigma &= 50ps \\ \mu &= 0.3ns\end{aligned}\tag{6.1}$$

In particular the average of the bell curve establishes at which time from the begin of the simulation the pulse is sent to the antenna, instead the standard deviation determine the shrinkage of the pulse. This means that if the  $\sigma$  increases also the duration of the pulse increases, and if it is enough large the requirements of pulse regime are lost, because differently from the continuous regime, in the case treated in this section the signals should be fast in order to improve the computational power.

In order to obtain a pulse it is necessary a signal that has values non null only in a short range of time. The Gaussian pulse is a good candidate because the Fourier transform of this function has the same shape of the initial signal. But the problem is that the components in frequency are dependent on the average  $\mu$  of the bell curve (they depend also on the  $\sigma$  but it is not an issue). This can be fixed by the fact that the modulating signal is carried by an oscillatory field: the peak of the Fourier Transform will be centered exactly on the frequency of the carrying signal. In this way it is possible to excite spin waves with the strongest frequency component that corresponds to that one chosen in principle for sinusoidal field. The last but not least advantage of the modulation with a Gaussian function is the following: the edge of the modulated signal are smooth and not sharp as it happens in rectangular pulse. This is a very positive point because it doesn't induce any issues in the magnetization dynamics as it will be discussed in the section 6.2. Hence the type of signal exploited in the simulation treated in this section offer the possibility to sent smooth signal in a certain moment of the simulation without taking care about the shifting of the signal spectrum in frequency space, and this is more advantageous when different set of inputs are applied in sequence, as it will be explained in the section 6.1.4. The concept described so far are illustrated in the figure 6.2. From the figure 6.2 (blue curve) it is clear that in pulse regime it is not possible to excite only one frequency in the waveguide, as it happens in the continuous regime. As it is will be explained in the next sections, the issues related to the other frequency components

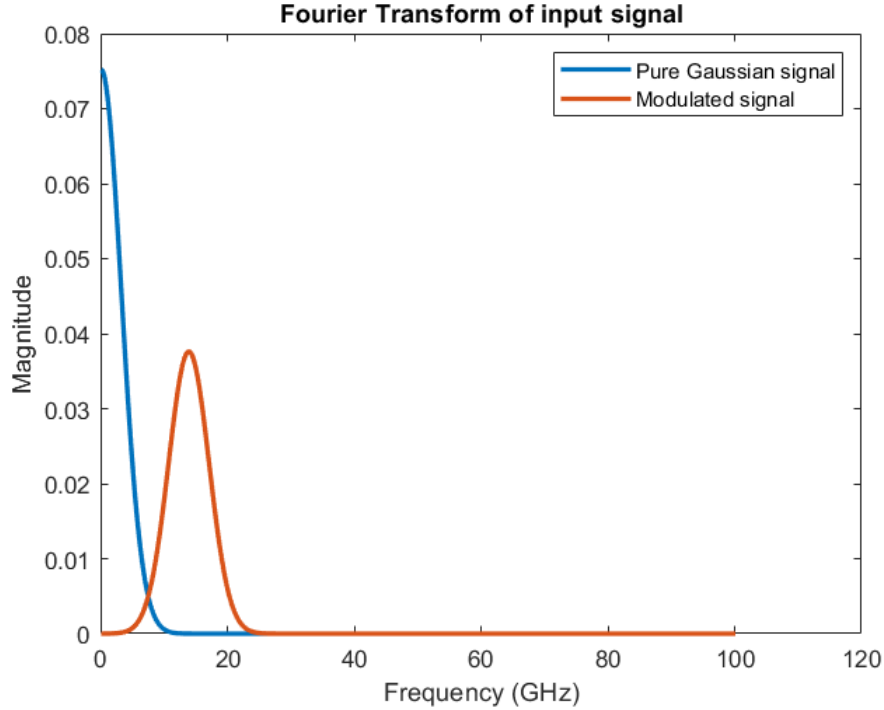


Figure 6.2: The plot represents the Fourier Transform of the Gaussian pulse and then the modulated signal by Gaussian pulse. As it is clear from the picture the same Gaussian is centered in different frequency values in the two cases, but it is required to be centered on a specific frequency so the blue curve is better.

are relevant and negatively influence the propagation of the spin waves.

### 6.1.1 One Input Propagation Analysis

The spin waves are excited by the modulated signal and the range of frequency components generated in the waveguide is more or less [2 GHz, 24GHz], with different magnitude, this means that their amount in the device is more or less relevant. The most important frequency is the one that corresponds to the peak of the Gaussian curve of the Fourier Transform. The main issue is that in the waveguide there is not only the required frequency

(13.82 GHz) but also the other frequencies included in the bell curve. Hence the propagation involves different wavenumbers. As a consequence for each wavenumber there is a specific lifetime, group velocity and decay length: this means that the spin waves generated by different frequencies interfere among them and they have to be taken into account in the interference pattern of the three inputs.

In order to analyze the propagation of one input in the waveguide, the simulation performed had the following setting: the antenna was placed at  $2 \mu\text{m}$  from the left edge of the device, as it happens in the continuous regime, the modulated signal parameter are reported in the equation 6.1, the damping profile is applied in the x direction dealing with the strategy described in the section 3. The signal doesn't start exactly at the begin of the simulation but after 0.2 ns: this is done to be sure that the signal applied starts from the lowest values in the left tale of the Gaussian curve. In this way the signal is symmetric respect to the right part of the curve, which corresponds to the side after the value corresponding to the average. The signal can be shifted in the time range, it is not an issue, but in this analysis the purpose is to observe the behaviour of magnetization when the signal arises and when it decreases following the two side of the Gaussian, hence for this reason that particular setting has been chosen. The signal starts to arise at 0.2 ns and return to zero at 0.5 ns, after following the bell curve. In the figure 6.3, the first two snapshots represents the magnetization when the signal is still on the left side of the curve, instead the third corresponds to the moment in which the signal is going to zero, and finally the last snap represents the magnetization after the end of the signal.

The maximum peak of the signal is reached at  $t = 0.38 \text{ ns}$ , indeed in the second snap the spin waves seem to be still intense, instead after overcoming this maximum, in the antenna position, the magnetization starts to decrease and in the last snap it goes to zero in the same position because the signal is already ended. Far from the antenna position the spin waves don't reach immediately the zero amplitude because they are not directly influenced by the applied signal and they continue to survey powered by the exchange energy between neighbouring spins.

In pulse regime, as it is clear from the figure 6.3, the amplitude of the magnetization (the z component is in the range  $\sim [-19 \text{ kA/m}, +19 \text{ kA/m}]$ ) is smaller than that one obtained in the continuous regime ( $\sim [-25 \text{ kA/m}, +25 \text{ kA/m}]$ ). Indeed in the pulse regime the amplitude of the signal needs to be

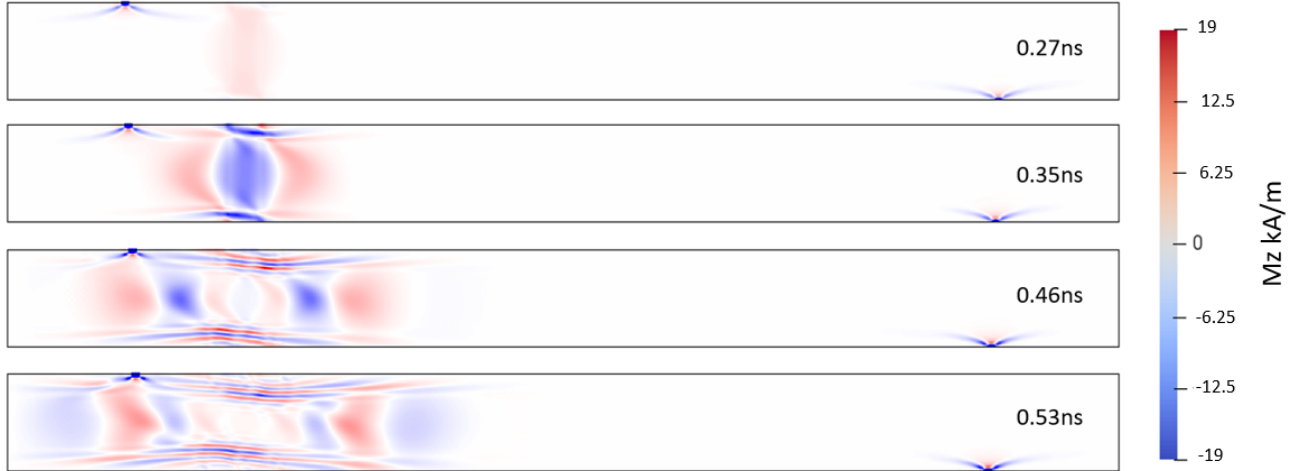


Figure 6.3: The snapshots captured in this image include the interval time of the simulation that goes from 0.27 ns to 0.53 ns. They represent the evolution in time of the component  $z$  of the magnetization.

stronger in order to excite the spin waves and to give them enough energy to survey in the waveguide, but the amplitude cannot be too high because non linear effects can occur in the dynamics of the magnetization. Hence generally speaking is reasonable the fact that in the pulse regime the spin waves are weaker than the continuous regime ones because the signal is shorter in time and for this reason would require an higher amplitude to reach the same effect of continuous regime but this is not feasible.

Furthermore also in this case there are the backward volume waves propagating from the edge. They should propagate in the  $x$  direction, but at the edge the initial magnetization is not exactly parallel to the  $x$  direction so it is proper defining the waves from the edge as intermediate waves between DE and BWV configuration. They propagate preferentially towards the centre of the waveguide and after  $\sim 0.8$  ns they reach the middle of the sample. When the signal applied goes to zero the dynamics of the magnetization starts to be very complex because all the components interfere with each other, hence it is not possible to realize a majority gate function anymore. This means that the output needs to be read as soon as possible otherwise the result disappear. Now the evolution of the spin waves propagation will be analyzed in depth in the figure 6.4.

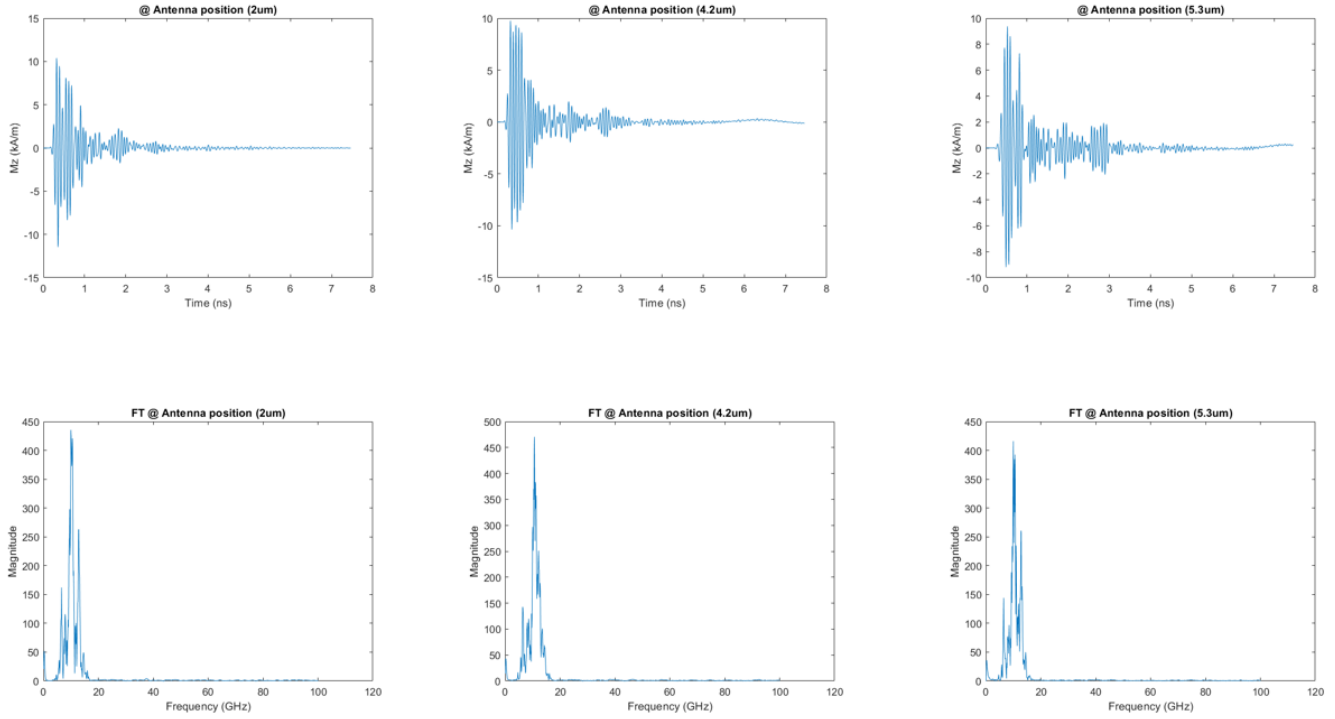


Figure 6.4: The signal is applied through the antenna at  $x = 2 \mu m$ , but the time spectrum of the spin waves and the spectrum of Fourier Transform are observed in space at different position. In particular the positions taken into account are  $x = 2 \mu m$ ,  $x = 4.2 \mu m$ ,  $x = 5.3 \mu m$ .

At the antenna position the magnetization in time assumes the same shape of the signal, but it is a little bit more spread out respect to the signal, indeed the input goes to zero at 0.5 ns but the magnetization reaches the lowest value at 0.65 ns before arising again. The spectrum of the Fourier Transform is similar to that one of the modulated signal, at least regarding the range of frequency, because regarding the shape is not so smooth as that one of the signal. This apparent incoherence is due to the fact that even if the input goes to zero and the magnetization should follow the signal, there are the intermediate waves that from the upper and bottom edge of the waveguide

reach the middle and they sum each other giving rise to a kind of excitation again, indeed in the figure it is possible to see that spins starts to precess again at 0.8 ns more or less but with a much lower amplitude up to disappear completely. The presence of the intermediate waves influences also the FT spectrum indeed there are peaks in the FT plot that are absent in the FT of the signal. Going far from the antenna there are two phenomena happening: first of all it is clear that a broadening of the magnetization spectrum occurs and then the spectrum of FT becomes lower, because far from the excitation point the spin waves are weaker, hence they have a smaller amplitude. The spectrum broadening of the magnetization becomes stronger and stronger as the point of view becomes more far from the antenna, indeed in the first row of the figure 6.4, proceeding towards the right side, the magnetization seems to be longer in time. This is due to the fact that in pulse regime different frequency components are excited and as a consequence each component has its own group velocity and its wavelength. Hence in the antenna position all the components are very close to each other because there they are just excited. Instead when they propagate the different group velocity starts to play an important role so the spin waves with a lower group velocity will reach later a certain position. For this reason the spectrum seems to be spread out.

Regarding the evolution in space of the spin waves it is necessary to analyze the Fourier Transform in space at different time as it has been done in the figure 6.5. The detection point taken into account in this plot are strategic because they allow to understand what happens in three different states of the applied signal: before and after the peak and at the peak itself. It is possible to deduce that as the time increases the FT spectrum changes respect to the initial behaviour that is quite similar to the Gaussian shape, with the maximum point corresponding exactly to the wavenumber related to the frequency used ( $k=6.28 \text{ rad}/\mu\text{m}$ ). This happens because at the begin the influence of negative effects is negligible, but in the other detected time intervals the intermediate waves become closer and closer to the center of the waveguide. Hence they interfere with the DE waves and for some wavenumbers the magnitude becomes lower because these components are killed by destructive interference. Furthermore as the time flows the components present in the waveguide separate from each other, far from the antenna, because of the different group velocities and this causes more interference pattern. Thereby the probability to have waves canceling each other is higher, indeed for this reason the yellow curve shows more negative peaks with regard to the other two curves.

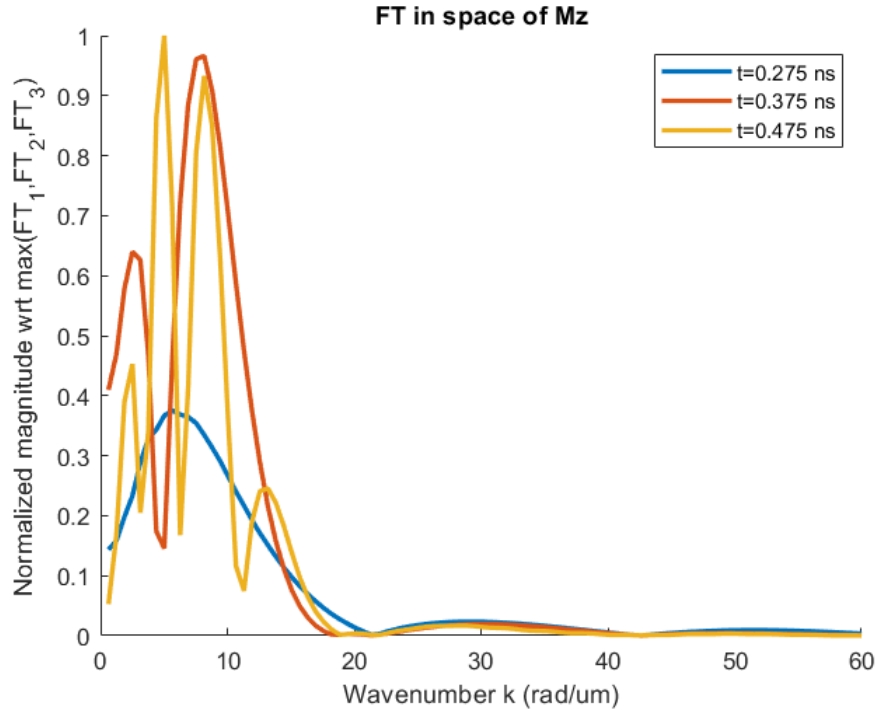


Figure 6.5: The signal is applied through the antenna at  $x = 2 \mu m$ , then the Fourier Transform is performed at several time interval, in particular for  $t = 0.325$  ns (before reaching the maximum peak of the signal Gaussian shape),  $t = 0.375$  ns (corresponding to the maximum peak of the signal),  $t = 0.475$  ns (near the end of signal, on the right side of the bell curve).

Even if a lot of group velocities are present in the waveguide, it is possible to know a general group velocity that can be considered as a weighted average of all components present in the sample: it was computed the time taken by the spin wave to reach the output (it is supposed to be at  $d = 3\lambda$  from the antenna) and then the velocity is obtained by the ratio between the space and the time. The result is  $\sim 4.28 \mu m/ns$ . It is not possible to obtain from the simulation in pulse regime the group velocity of a single components, but it is clear that the result obtained is mostly determined by the components that in the Fourier Spectrum show an higher magnitude.

In the section of Continuous Regime a method to attenuate the interme-

mediate waves from the edges has been described. In the case of pulse regime an alternative method will be described, but it is equivalent to the other one and they interchangeable. In order to eliminate the intermediate waves it is possible to make the magnetization in the waveguide more uniform. As it has been already explained in the section 3, when an external field is applied in order to align all the spins, avoiding a random magnetization, the effective field present at the edges of the waveguide is weaker because of the demagnetization field. So the solution is to compensate the external field in order to have in the waveguide the required value. In this way it is possible to attenuate the non uniformity at the edge as it is clear in the figure 6.6: in the snapshot representing the uniform case the intermediate waves are almost absent, instead in the non uniform case they already start to propagate towards the center of the waveguide.

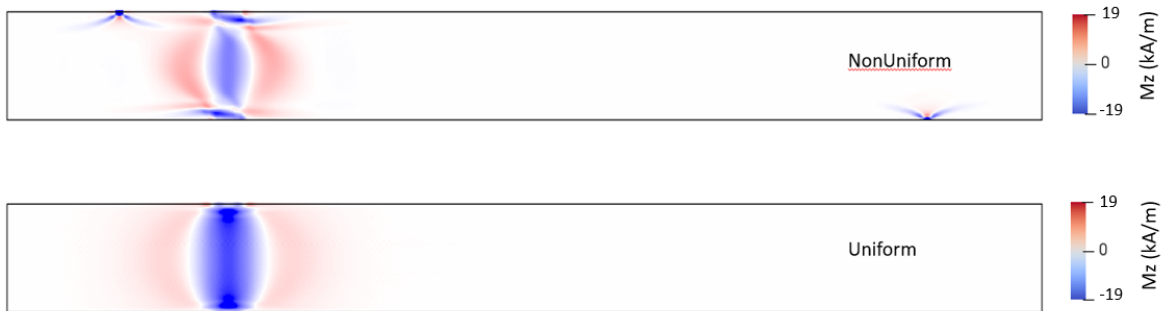


Figure 6.6: The two snapshots represents the uniform and the non uniform case. The first one has a scale for reduced magnetization, hence it is computed for unit length, instead the second one represents a non normalized magnetization so it has a different scale. But this doesn't matter, it's only a scale factor. They are captured in the same moment.

This uniform condition is ideal and it is not possible to obtain it in the real world, because the demagnetization field cannot be compensated as easy as in the simulation. Indeed the demagnetization field is not a constant value but depends on the position in the waveguide, hence there is no way to apply an external field dependent on  $x$ ,  $y$  and  $z$  direction. But the main reason is that the shape anisotropy is a natural consequence of the confinement of the structure. Hence even if a very large external field is applied, demagnetization will be still present, but for sure it will have lower values. In this case

non linear effects could arise in the system. The only feasible solution is to build a larger waveguide: in this way the intermediate waves need an higher interval time to reach the middle and to interfere among them. But in this scale the nanoscaling requirements fail.

Anyway in the pulse regime the other big issue is the fact that there is not only one frequency component and this makes everything more difficult. So far there is no method to fix this last problem.

Either in the uniform and non uniform case the output is readable up to the intermediate waves reach the result detection window, because starting from that moment the dynamics becomes too complex and it is impossible to see the regular phase alternation. If it is supposed that the output window is far from the input a quantity equal to  $3\lambda$ , in the non uniform case the magnetization is readable up to  $\sim 1ns$ , instead in the uniform case the output is good up to  $\sim 2ns$ .

### 6.1.2 Interference Pattern Analysis

As already done for the continuous regime, also in the case of the pulse regime it is necessary to analyze the interference pattern with at least two other inputs, in order to demonstrate the realization of the majority gate function. In this section the device taken into account has three inputs: this means that three antennas are applied to the waveguide and the signal sent to the port are sinusoidal Gaussian modulated, as it has been discussed in the section 6.1.1. In this dissertation for the pulse regime the configuration taken into account is the following: the antennas are placed always at the same distance from each other that corresponds to a multiple of the wavelength ( $d = n\lambda$ ,  $n$  is chosen equal to 1). Then in order to obtain the phase 0 or  $\pi$  of the magnetization it is sufficient to change the phase of the applied signal. As already it has been said in the previous chapter, in the real world it is not easy to implement this method because the phase at the input is not exactly as it is required but it changes due to the propagation of the signal in the wire. Hence it necessary to tune the input phase through the phase seen at the output. The strategy used to implement the majority gate in the continuous regime is not applicable in the pulse regime, because when the output is read, the input could be already extincted. Anyway this goes beyond the purpose of this work, hence here the attention is focused in analyzing by the simulations what happens in the waveguide.

If more than one inputs are applied the situation is the following: each input excites spin waves with several wavenumbers and group velocities, then all the components of one input interfere with the components of the other two inputs. Now it will be analyzed first the case where all the inputs have the same phase, for example  $\pi$  (bit 1). Hence the following configuration will be performed:  $I_1 \rightarrow 1$ ,  $I_2 \rightarrow 1$ ,  $I_3 \rightarrow 1$ . This is the easiest possible case together with its complementary  $0\ 0\ 0$ , because the spin waves are always perfectly in phase so constructive interference occurs, with the highest intensity of the magnetization. In order to read the output it is necessary that all the inputs reach the detection point. If the distance among the antennas is the minimum possible ( $d = 1 \cdot \lambda$ ) the output should be at least  $d = 3 \cdot \lambda$  from the first input, that is the most critical one. This means that if the spin waves have the group velocity computed in the case of one input propagation ( $\sim 4.28 \mu\text{m}/\text{ns}$ ) they spend 0.7 ns to reach the output, hence it is required to wait at least this time before reading the correct result. Furthermore the reading time has also an upper limit because if the signal extinguish after 0.3 ns, the spin waves are not constantly powered and then when the intermediate waves come from the edge the DE waves have no enough energy to keep alive and the dynamics becomes understandable. In the figure 6.7 it is clear that the output is readable when the intermediate waves by now reached the middle of the waveguide, hence the range in which the result is still correct is [0.7 ns, 0.95ns]: it is a 0.2 ns interval. In the one input case instead the output is readable in the range [0.7 ns, 1.6 ns]. Hence if there is only one input the output can survey longer and this sounds reasonable because the probability to have complex dynamics is lower, since the source of intermediate waves is only one and the total number of frequency component is smaller than three input case.

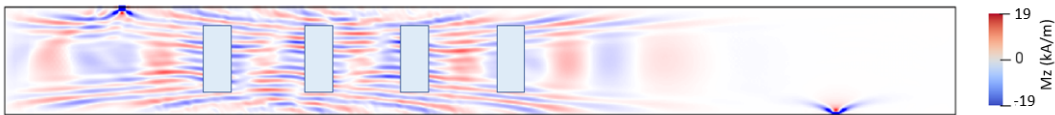


Figure 6.7: The snapshot is captured 0.7 ns in order to be sure that all the inputs reached the output. The configuration sent in the majority gate is 1 1 1, indeed the input are blue (1) and the output is also 1 (blue).

In order to analyze what happens in the waveguide with three inputs it is

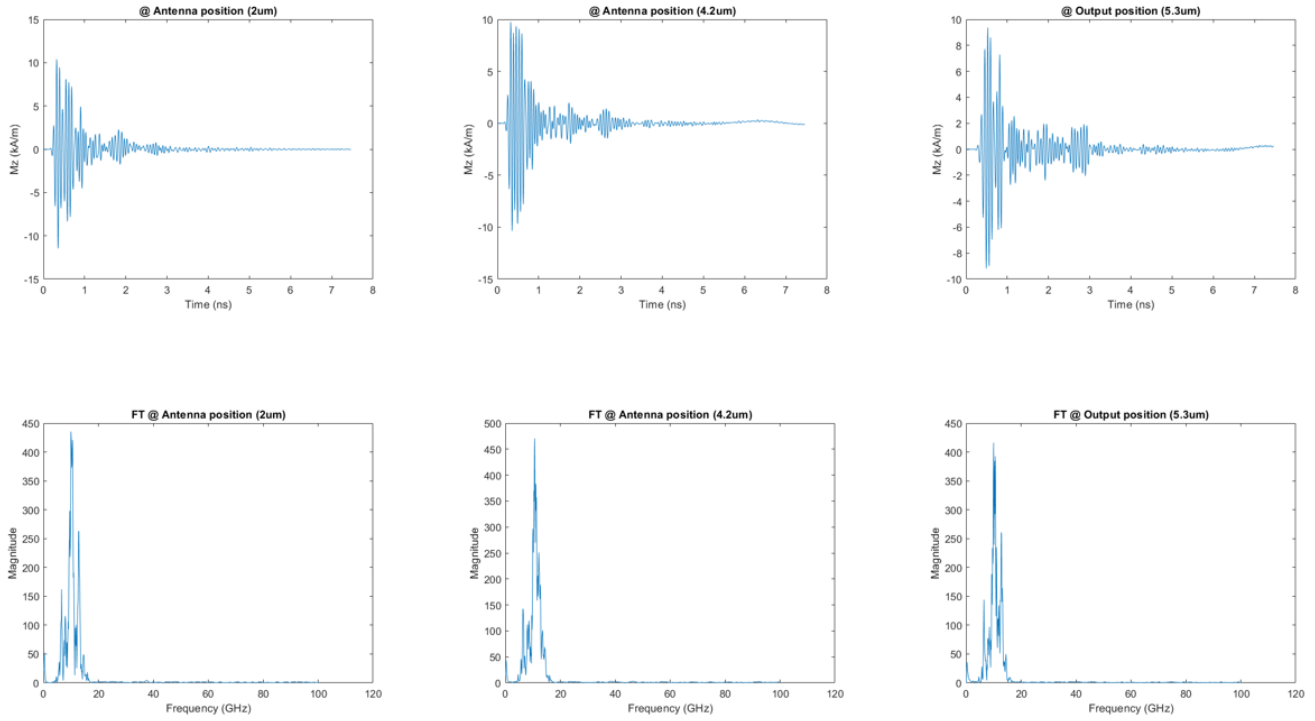


Figure 6.8: The plots represent the magnetization in time and the Fourier Transform at antennas position and at the output. In particular the points in the waveguide taken into account are: the first antenna ( $2 \mu\text{m}$ ), the third antenna ( $4.2 \mu\text{m}$ , far  $2 \lambda$  from the first input) and the output at  $5.3 \mu\text{m}$  ( $3 \lambda$  from the first antenna).

necessary to look at the magnetization in time and at the Fourier Transform, since the first one describes the broadening of the spectrum and the last one describes the frequency components. In the figure 6.8 the points taken into account are the same as that ones described in the case of one input propagation, in order to compare the two case. If there are more than one input in the waveguide, the magnetization in time is subjected to a relevant broadening of spectrum in each position considered. Differently from one case, where at  $2 \mu\text{m}$  the broadening is more or less negligible, in this case also at  $2 \mu\text{m}$  there is an evident spreading out in time: this is due to the

fact that when an antenna excites spin waves, they propagate towards the left and the right side of the input. Hence this means that in every position there is the overlapping of the spin waves coming from all the antennas with their several group velocities. In the figure 6.9 it is possible to visualize the influence of each antenna on the other antennas position. As it is clear from the sketch a certain position receives a stronger influence from the antennas closer to it, but there is also the impact of the antennas further from the position considered even if in this case the influence is weaker.

A stronger or a weaker impact from one antenna on another is determined by the amplitude of the magnetization when it reaches a certain position. Hence it is obvious that if a position is far from the excitation point, when the spin waves arrive a phenomenon of decaying has been occurred, because of the damping that kills slowly the spin waves as the time flows and as the distance from the input becomes greater. For this reason, looking at the figure 6.8, in all positions taken into account the broadening of the spectrum is the same, indeed it is possible to see the spin waves up to 3 ns in each position, but the intensity of the spectrum is different and it reflects perfectly the concept expressed in the sketch 6.9 (here the case of the 0 0 0 configuration has been represented), indeed dealing with this hypothesis the greatest intensity should be, in this case, that one of the second input and the plot in the figure 6.10 confirms this idea. For the other inputs configuration, the concept expressed above is valid but the greatest intensity could be attributed to a different position, depending on the constructive or destructive influence received.

So far only the simplest inputs configuration (1 1 1) has been described. The theoretical working of the majority gate is more or less the same for all combinations of inputs, but in the cases in which the result is the same, such as 1 1 1 or 1 0 1, the amplitude of the magnetization is not the same, and also concerning the phase there will a certain shift between the two cases. The reason is very simple: for example the interference among three inputs with value 1, has the maximum amplitude and the maximum phase because all the inputs are equal, but if the interference occurs among three different inputs (1 0 1) the result is always one but instead to be determined by two constructive interference, they are one constructive and one destructive (this condition is called weak majority). Hence the amplitude of the bit one is weakened and the phase is a value around  $\pi$  but not exactly. The same phenomenon has been explained already in the section about the continuous regime, but in this case it is a little bit more complex because when the

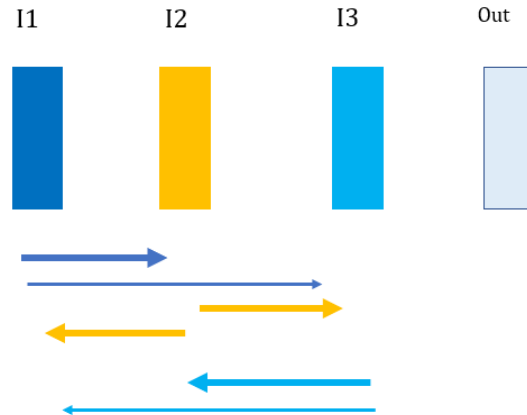


Figure 6.9: In the sketch the arrows represent the spin waves coming from a certain position. The marked line indicates a strong influence of a certain antenna on that one considered, instead a fine line indicates a lighter impact.

output is readable (0.7 ns) the inputs signal is already gone to zero (0.5 ns), so the spin waves are not powered anymore and it is very easy for the system to acquire undesired shift on the output, in particular way when the inputs are different among them (1 0 1 in the case described here). In the snapshots taken from the simulation is hard to distinguish red and blue, which corresponds to zero and  $\pi$  phase. Hence in order to read the output a trick has been exploited: from the simulation with one input, supposing that it has the value 1, it was obtained a reference signal with a certain phase  $\phi$  that corresponds to the bit one. Then this reference signal was overlapped on the plot of the magnetization respect to the time (extracted at the output). In this way it is clear that, if the plot of the magnetization is in phase with the reference signal, the result at the output corresponds to one, as it is expected from the truth table of the majority gate.

As it is understandable from the figure 6.11 the output is readable in a small time range equal to [0.88 ns, 1.09 ns]: before it is not possible to read the output because the first input isn't arrived yet, and after this range a shift in the phase occurs because of the complex dynamics.

Regarding the different amplitude and phase in the cases that theoretically

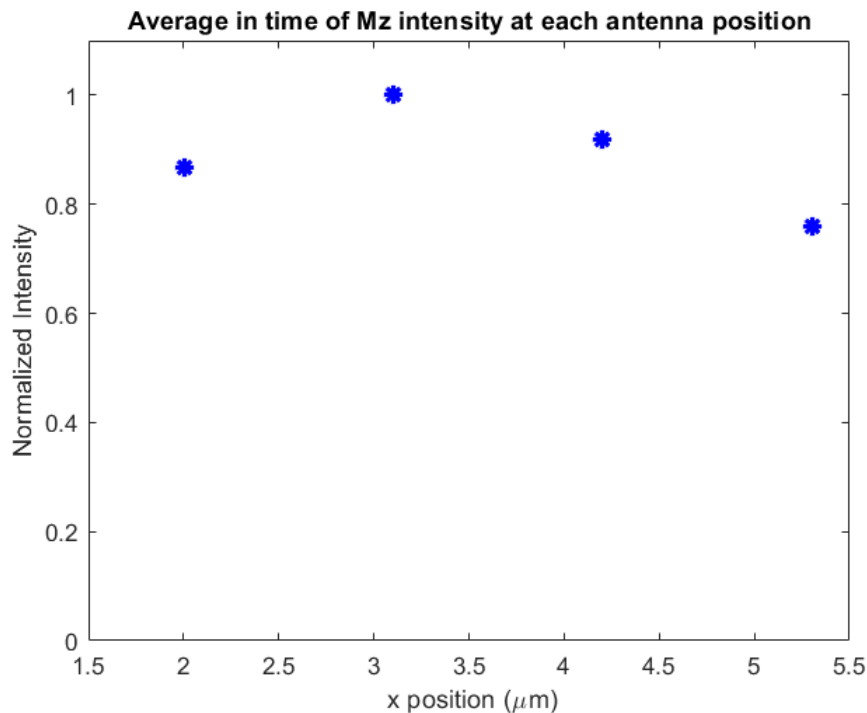


Figure 6.10: The plot shows the average value in time of the magnetization at each antenna position and at the output. As it has been predicted, at  $x=3.1 \mu\text{m}$  the intensity magnetization assumes the highest value, because this position is the only one that has the minimum distance from two antenna, rather than from one as it happens for the other points. In this case the configuration corresponds to 0 0 0.

should give the same result, a comparison is reported in the figure 6.12 between the two configuration described so far: 1 1 1 and 1 0 1. In the figure it is clear that the average magnetization amplitude of the 1 0 1 configuration is a little bit smaller than the other one, and the phase of 1 0 1 is more or less the same to the phase of the result from 1 1 1, even if there is a small shift. Hence the value 0 and 1 are represented by a range of phase values not only one, and thresholds are necessary in order to distinguish them. In the section of the continuous regime the image reported in 5.10 explains very well the concept (it is valid for either continuous and pulse regime, even if the threshold values can be different ): the same image is not available for

pulse regime yet because no experiments are performed in this sense so far.

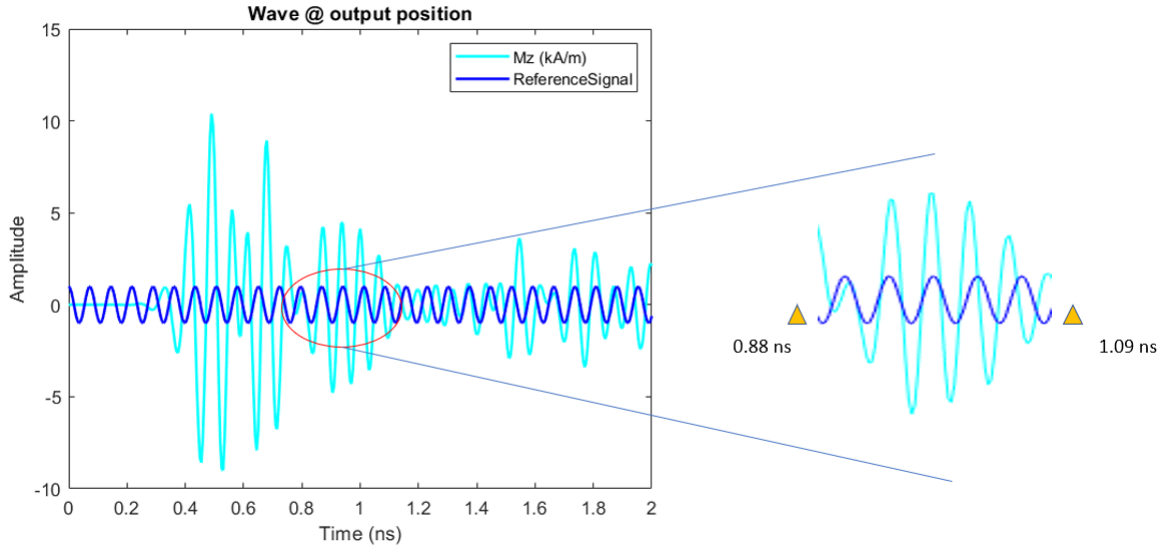


Figure 6.11: In the figure is reported the magnetization in time at the output, resulting from the configuration 1 0 1. The zoom is done in the time window where the result is correct and it is in phase with the reference signal.

### 6.1.3 Shrinkage of the Gaussian Modulating Signal

So far the Gaussian modulating signal used to excite the spin waves has a width equal to  $\sigma=50$  ps. But in order to increase the speed of the computation it is necessary to exploit narrower signal, because in this way, theoretically, it is possible to increase the throughput. As it happens also in the CMOS electronics, the bottle neck is due to the intrinsic characteristics of the devices, since they have physical limitations that, in the case of spin waves applications, prevent them to follow in a proper way the excitation signal. In an ideal case delta of Dirac should be used in order to have the possibility to send as much as possible signals in a certain time interval. But there are two main issues in a spin wave based device: first of all, even if the excitation signal is very narrow the next signal cannot be sent before spin waves have been reached the output window, otherwise the result of the operation

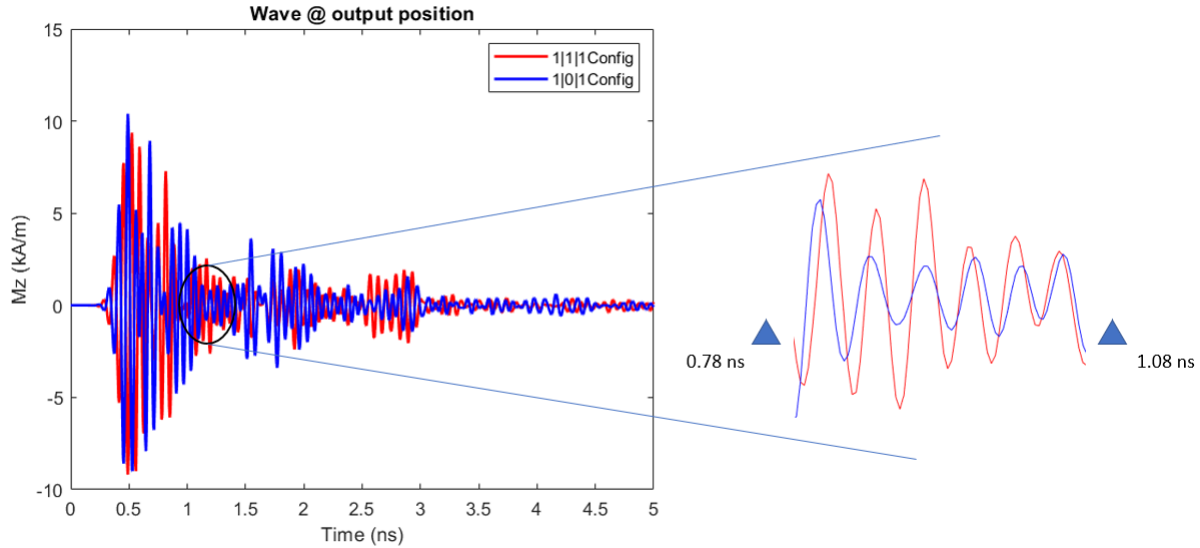


Figure 6.12: The magnetization in the plots is extracted at the output for both cases. The zoom shows the small shift between the two plots in the time interval where the output is correct.

is lost. Hence the critical parameter is the speed of spin waves, because if they were faster they would reach the output in shorter time and thereby they would have no need to be powered by the excitation field for long time. Consequently the excitation signal could be narrower. The second big issue is the following: according to the properties of Fourier Transform indicated in the equation 6.2 if the signal is compressed the FT is stretched, hence this means that the components in frequency in the waveguide is increased (figure 6.13). This consequence implies that interference mechanism becomes more complex and the broadening of the spectrum get worse because other wavenumbers are added to the system, and then the time interval in which the result remain correct is reduced, supposing that it is able to reach the output in the proper way. Several simulations are performed in order to understand which is limit of shrinkage for the excitation field and the value obtained for the width of the Gaussian modulating signal is  $\sigma = 15$  ps: in this case the output is readable for only 90 ps, and after this time it doesn't follow the interference pattern anymore, because intermediate waves from the edge take over.

$$\mathcal{F}[x(at)] = \frac{1}{a} X\left(\frac{\omega}{a}\right) \quad (6.2)$$

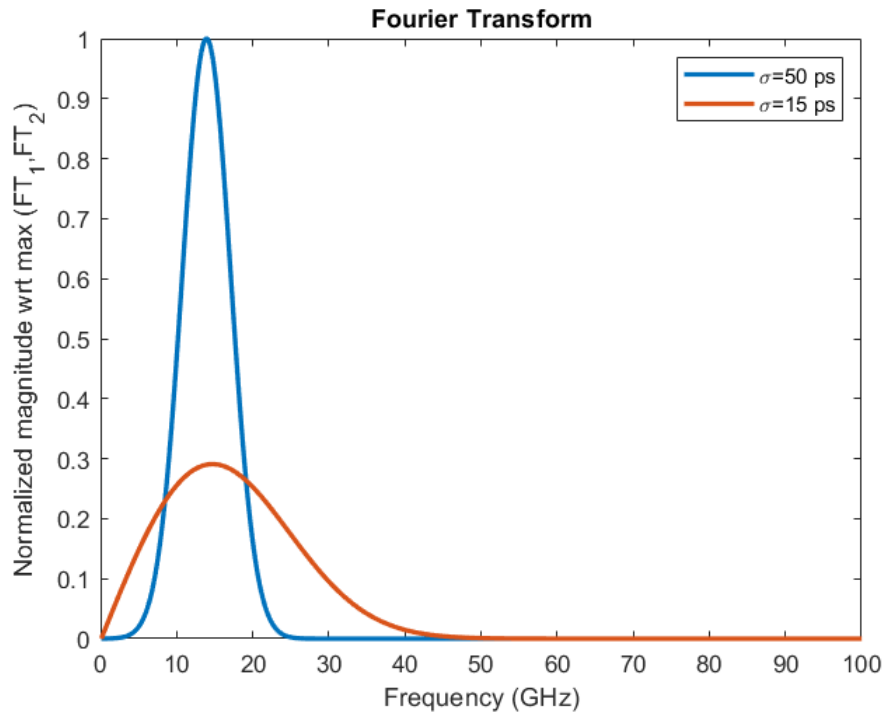


Figure 6.13: The Fourier Transform has been performed for the normal and shrunken signal. The last one has the same parameter of the first signal, it changes only the value of the width, that determines the compression of the Gaussian modulation.

#### 6.1.4 Repetition Rate

So far only the working operation of the majority gate has been analyzed, but it is not enough. Indeed a good electronic device has to be able to process data in repetition with a very small delay between consecutive set of inputs. In this section the capability to read different output coming from successive inputs will be described. The setting of the simulation is reported in the

	Configuration	I1	I2	I3
1 <sup>st</sup>	0 1 0	$A \sin (2\pi ft)k_1$	$A \sin (2\pi ft + \pi)k_1$	$A \sin (2\pi ft)k_1$
2 <sup>nd</sup>	1 1 0	$A \sin (2\pi ft + \pi)k_2$	$A \sin (2\pi ft + \pi)k_2$	$A \sin (2\pi ft)k_2$

Table 6.1: The table represents the simulation setting of inputs configuration for the two set of bits sent consecutively.

table 6.1. The parameters in the table 6.1 are described in the equation 6.3.

$$\begin{aligned}
 A &= 3mT \\
 k_1 &= \exp\left(\frac{-(t - \mu_1)^2}{2\sigma^2}\right) \\
 k_2 &= \exp\left(\frac{-(t - \mu_2)^2}{2\sigma^2}\right)
 \end{aligned} \tag{6.3}$$

The two set are characterized by two different Gaussian modulating signal: it has the same width in both cases but the average  $\mu$  changes because the two set need to be applied in successive moments, hence in the simulation changing the average, the signal for the same input can be sent as a sum of the two modulated fields. In the figure 6.14 it is shown how the signal for the same input looks like with regard to the time. Obviously in the reality the input cannot be a sum of the two Gaussian modulated signals, because in this case the FT is totally different from the expectations. This is only a trick used in the simulation to represent the consecutive signal, but they have to be considered as two separated signals. There is an important rule to be respected when consecutive signal are applied: the average  $\mu$  of each signal has to be a multiple of the carrying signal period ( $T_s$ ). In this case the period of the carrying signal is 72.36 ps, indeed the average of the first set signals ( $\mu_1$ ) is equal to 0.3618 ns ( $5 T_s$ ) and the average of the second set signals is 1.2301 ns ( $17 T_s$ ). In this way the successive signals are always applied with the same phase, if they represents the same bit, or with a phase shift equal to  $\pi$ , if they are complementary; hence this method guarantees that no additional phase shift is introduced between consecutive signals due to the wrong position in time of the second signal.

Furthermore the second set of inputs needs to be applied after the time interval necessary to read the first result. From the previous calculations it

is known that the result can be read at the output more or less after 0.8 ns from the input entry. Hence in the best case the second set should be applied just after  $\sim 1$  ns from the first set, in order to guarantee that the first result will not be lost. According to the expectations the frequency at which the inputs can be changed to compute different operations should be  $\sim 1$  GHz: this is the value obtained from the previous hypothesis, but it is only an approximation. The sets chosen to test the repetition rate are not just

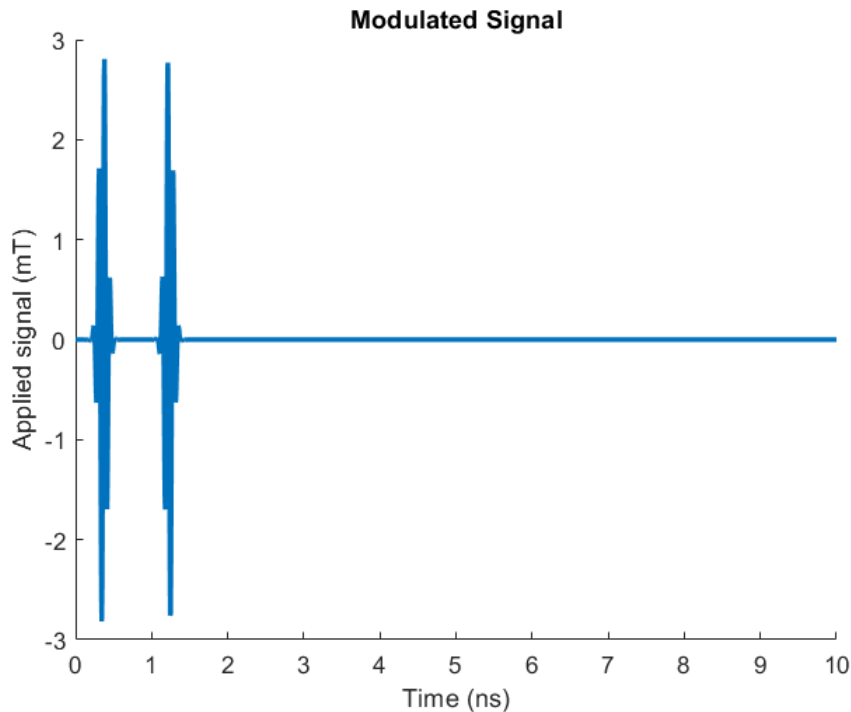


Figure 6.14: In the plot the two successive Gaussian modulated signal are shifted by a quantity equal to  $\pi$  so they represent the two complementary bit values.

random: these two configurations should give opposite results, hence in this way it is possible to understand how fast is this majority gate to switch the output, supposing that the inputs are applied following the described rules. In figure 6.15 it is shown the status of the magnetization if two signals

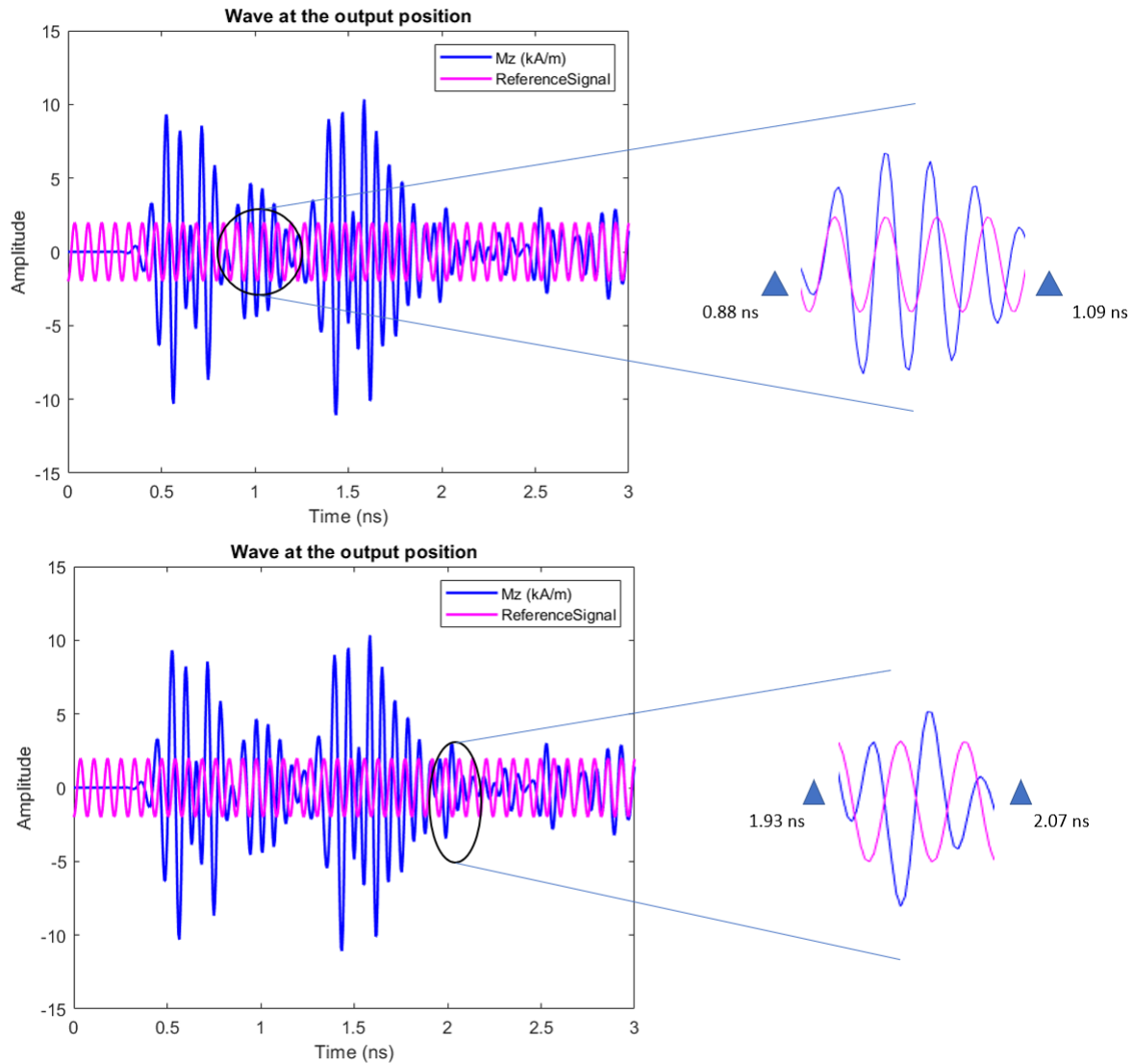


Figure 6.15: The reference signal has the same phase of value 0, this means that if the result of the operation is 0 it is in phase with the reference (first zoom), instead if the result of the input combination is 1 it is shifted respect to the reference of a quantity equal to  $\pi$  (second zoom).

are applied in sequence: in the time interval [0.88 ns, 1.09ns] the result of the first set inputs is valid, then the spin waves are excited again by the second

set of inputs, and the result of this second operation is readable in the range [1.93 ns, 2.07 ns]. The time necessary before reading the output is the same in the two cases, even if in the second one the first result has to be overwrite. Nevertheless, this is not a big issue because when the second set starts the spin waves generated by the first one are weaker than the new waves, hence there is no problem to cancel the first result. Even if it is possible to read the second result, the time in which it remain valid is smaller than the time of the first result, as it clear comparing the two obtained range: for the first set is  $\sim 0.21$  ns for the second instead it is  $\sim 0.13$  ns. This is reasonable because when the second inputs signals go to zero the spin wave are not powered so they becomes weaker and weaker and they have not enough energy to dominate on the residual spin waves from the first set, hence they interfere and the result cannot be read anymore. Furthermore in the figure 6.16 it is possible to see that the range of wavenumber components in the waveguide is the same between the two set, but the interference pattern is a little bit different because the height and the position of the peaks change in the two plots.

## 6.2 Rectangular Pulse Excitation

Even if in the simulation the excitation with a modulating Gaussian signal and a carrying frequency works well, in the reality a logic gate has to operate with signals more similar to step function. Hence in this section the spin waves based majority gate with a rectangular pulse excitation is described. The working principle in this case is the same as that one already deduced for the Gaussian pulse, thereby here the analysis is more focused on the comparison between the two cases.

The signal exploited here has no carrying frequency hence the Fourier Transform depends only on the duration of the pulse. Premise that the main frequency component should be 13.82 GHz, as explained in the section 6.1, if the width of the pulse increases the magnitude of the undesired component decreases, but also the magnitude of the wanted frequency decreases. Instead if the width of the pulse decreases, the magnitude of the frequency component increases. Hence a trade off is necessary to satisfy some specific requirements: the magnitude of the desired frequency component should be enough great respect to the other components, and at the same time the

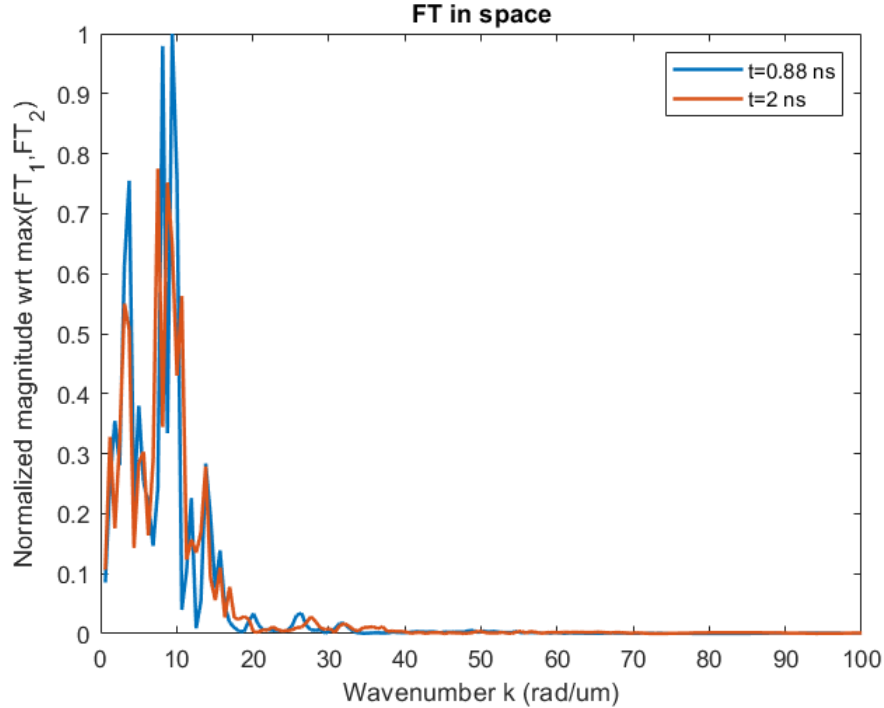


Figure 6.16: The Fourier Transform in space was computed in different moments: the blue curve corresponds to the time when only the first set generated spin waves are present, instead the orange curve corresponds to the time in which spin waves generated by the second set are present and interfere with the residual waves coming from the first set.

unwanted frequencies should be attenuated as much as possible in order to avoid the broadening of the spectrum and interference among waves with different wavenumber. Taking into account these assumptions and looking to the figure 6.17, it is clear that the best option is the rectangular pulse with a width of 20 ps: the magnitude of the frequency component 13.82 GHz in this case is only a little bit smaller than the other cases, but the magnitude of undesired components are much smaller than in the rectangular pulse with  $\sigma = 50ps, 100ps$ .

The amplitude of the applied signal is 3mT as in Gaussian pulse cases, and three antennas are applied in order to implement the majority gate function. The configuration tested in the simulation is 0 1 0. Since with rectangular

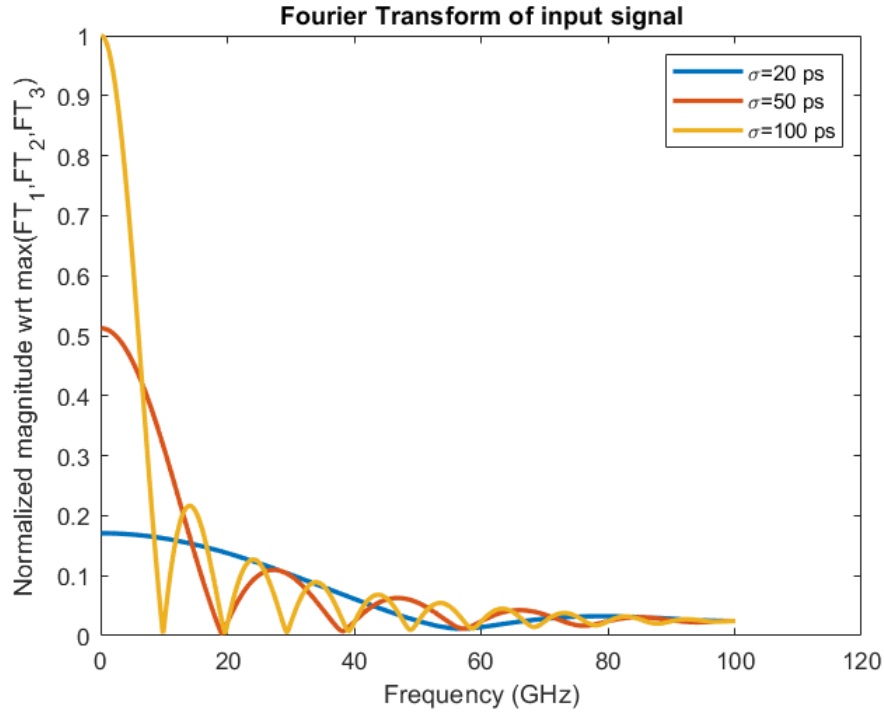


Figure 6.17: The plots represent the Fourier Transform of rectangular pulse with different width, in particular three values are present in the figure:  $\sigma = 20ps, 50ps, 100ps$

pulse the duration of the excitation is only 20 ps, against the Gaussian excitation that it is 340 ps, the spin waves at the output after 0.78 ns (the time necessary to wait before reading) are weaker in intensity respect to that one seen in the section 6.1 and the output is also readable for a smaller range. In the figure 6.18 is reported the result of the operation, and as it is clear from the zoom, in the time interval taken into account, the output is valid only from 0.9 to 0.98 ns. Hence the output is readable in a smaller range respect to the Gaussian pulse, due to complex dynamics that overcome than regular propagation of the DE spin waves.

In the figure 6.19 it can be observed that the Fourier Transform of the magnetization is not centered on the component frequency desired, because the

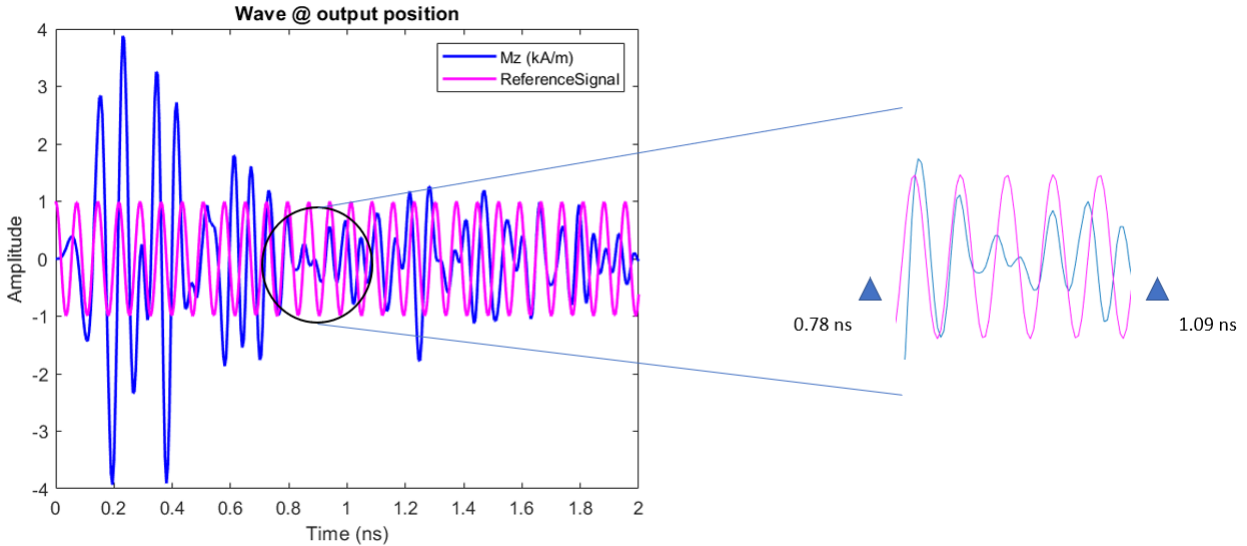


Figure 6.18: The output plotted represents the result of the 0 1 0 configuration. The reference signal has the phase of the value 0, hence it can be considered  $\phi = 0$ , because in this dissertation this phase value has been assigned to the bit 0.

rectangular pulse has that component but with a lower magnitude respect to the lower frequency components. Then the magnetization in time, seems to have the same decaying already obtained for the Gaussian pulse, even if the excitation signal is much narrower, indeed in both cases the magnetization reaches a very low intensity around 1 ns, before the arrival of the intermediate waves that make magnetization arising a little bit, without reaching the amplitude got in the moments when signal is still present. The fact that the magnetization decays in the same way in the Gaussian and rectangular case can be explained in different ways, in the following the most suitable points of views will be reported. In the case of Gaussian pulse, the signal is smoother than in the rectangular pulse, hence the magnetization can follow the signal because it is not so sharp and then the spin can adequate their precession mode to the change in the excitation signal. Instead in the rectangular pulse case when the signal goes from high to low value, being a step function, the change is so fast that the spin cannot immediately follow the signal, hence

they take a certain time interval to attenuate the precession movement. For this reason in the figure 6.19 the magnetization decays slower than the signal, and it is similar to that one of the Gaussian pulse. The other way to interpret this phenomenon is: the lifetime of the spin waves is independent from the excitation signal, if the pulse is much smaller than the lifetime, thereby the decaying is the same in both cases and the magnetization attenuates its amplitude of a quantity equal to  $\sim 30\%$  respect to the amplitude at the begin (when excitation signal is just sent).

Furthermore this observation can be supported by the fact that the mag-

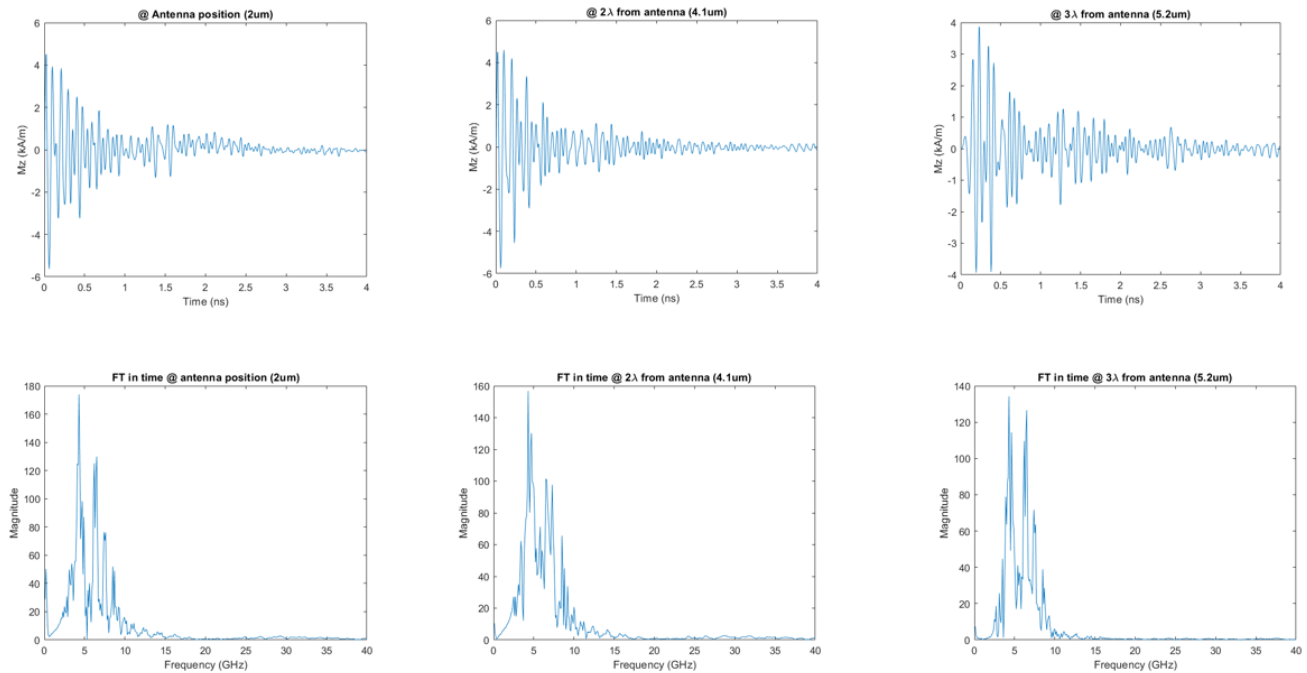


Figure 6.19: The plots represents the evolution in time of the component z of the magnetization, and the Fourier Transform in time at relevant positions: the first and third inputs and the output.

netization seems to decay in the same way with other type of signal, such as a quasi rectangular signal, which is constant up to a certain time and then it assumes an exponential behaviour. Despite this fact, it has been

demonstrated that the lifetime is not independent from the excitation signal, because if the energy pumped in the system increases the lifetime of spin waves decreases because the Gilbert damping factor increases due to the electron-phonon scattering [26].

Even if the decaying between the Gaussian and the rectangular pulse seems to be similar, the difference between the two cases are not negligible. First of all the Gaussian case treated in this dissertation is more efficient from computational point of view, because the output is more readable in terms of time window and intensity. Indeed in the figure 6.20 it is clear that the intensity of Gaussian pulse is much stronger than that of the rectangular case. This happens because if the signal is narrower, the system is powered for less time, hence the spin waves attenuation is stronger, even if the decaying behaviour is the same, indeed only the scale factor is different between the two case, regarding the intensity of the magnetization.

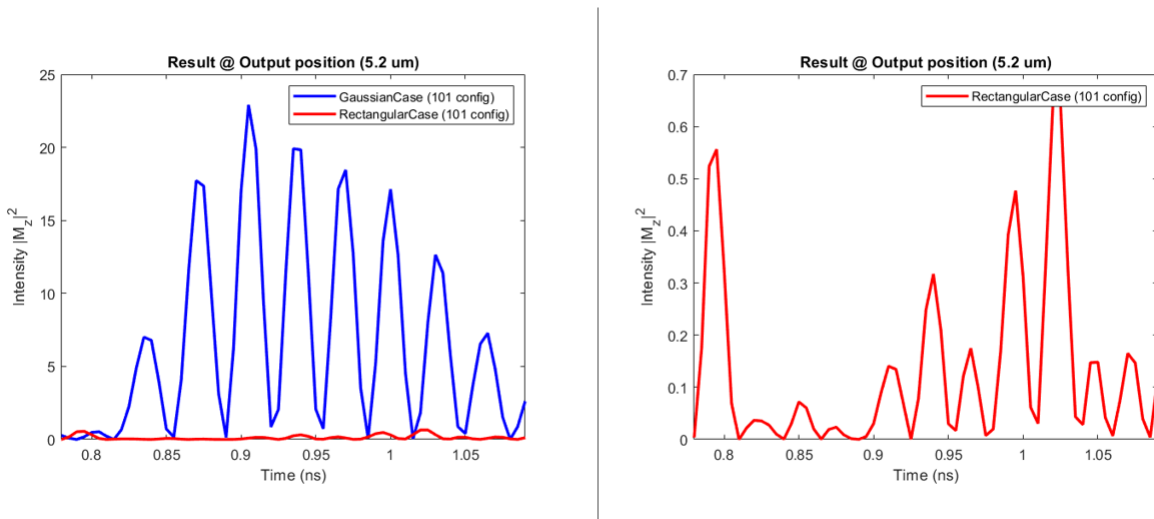


Figure 6.20: In the plots the intensity of magnetization  $m_z$  is represented as a function of time. The time window chosen on the x axis is corresponding to that one in which is possible to read the output.

# Chapter 7

## Conclusion

The main goal of the study carried in the thesis was to determine the behaviour of the spin waves in the propagation inside the system corresponding to the majority gate device, and to verify the correct working of the logic function. The dispersion relations are computed by both numerical and analytical method. The analytical equation used for the purpose don't take into account the demagnetizing field, so it is necessary to adopt some approximation on the applied field, in order to obtain a situation similar to that one performed during the simulation. Indeed in the software Mumax3, is implemented the computation of the demagnetizing field, hence the resolution of the LLG equation is carried taking into account not only the external applied field, but also the field generated by the material itself. If a fitting is performed between numerical and analytical dispersion relations, it is possible to see that in the majority gate both DE and BWV waves are present. Technically the majority gate should work in DE geometry, but also BVW waves appear. This is a drawback due to the demagnetization field and to the anisotropy that originate at the edge of the sample. If the waveguide is in a uniformly magnetized condition (quasi ideal situation), the BWV waves from the edge are attenuated but they are still present because the anisotropy cannot be eliminated, and this suggests that it is a real physical limits of the device. The presence of two different geometry in the system, makes more hard the correct working of the logic operation because unwanted interferences take place.

For the majority gate application is very important the determination of the lifetime, since it is necessary to understand how long the spin waves can survive before being subjected to a relevant attenuation, with bad consequences

on the output reading. In the case of "inline" layout of inputs, this parameter has much more importance because before reading the output, there is a certain delay, in order to be sure that all inputs have reached the output and have interfered among them. The computation of the lifetime is performed in the uniformly magnetized case, both numerically and analytically. In this way it is possible to extrapolate a more reliable value for lifetime, because the purpose is to know the lifetime of the DE waves only and doing like so, it is possible to attenuate the BVW waves from the edges. The determination of the group velocity is useful because it suggests how fast interference at the output window occurs and it gives an idea about the interval time to be waited before reading the right result.

After the first part about the characterization of the spin waves in the majority gate structure, in the next section continuous regime mode has been analyzed. In order to see the basic evolution in the device of the spin waves, only one input has been applied and some issues has been revealed, related to the reflections from the edges, then in a second moment two other inputs have been applied and interference pattern has been explained, with the related consequences. In this case a sinusoidal field is exploited, with a specific frequency, which allows to have a good trade off between power consumption, excitation efficiency and at the same time yielding a proper wavelength for the waves. The main issues in the continuous regime are the intermediate waves generated from the shape anisotropy at the boundary of the structure, and the different amplitude of the spin waves generated by the three inputs. This mismatch is due to the fact that the inputs have different distance from the output, hence the waves are subjected to the attenuation in different way. Then the concept of strong and weak majority is demonstrated: the input bit configurations, giving the same bit value as result, don't correspond to the same value of magnetization amplitude or magnetization phase respect to the reference signal, hence threshold values are needed to distinguish the bit 1 or the bit 0.

Successively pulse regime has been modelled with two different input signals: the Gaussian field with a carrying frequency and the rectangular field. One can find that there is huge difference between the continuous and pulse regime, since in one case the spin waves are continuously excited and only one wavelength is provided by the inputs, hence the only limitation is given by the unwanted interference between DE and BVW waves. Instead in the other case, after a certain time interval the spin waves are not longer fed, and furthermore different frequency components are excited, if one has a look at

the Fourier Transform of a pulse signal, hence also the spectrum broadening occurs in pulse regime. The main consequence is that there will be an additional contribution to the interference pattern given by the superposition of the spin waves with different wavelengths. Besides the spin waves lifetime now has a greater importance rather than in continuous regime, since in this case the inputs disappear after pulse duration. This means that the output reading has more restrictions. In particular, for Gaussian modulated signal case, the shrinkage of the Gaussian modulating signal is performed in order to find the limiting signal width at which spin waves can be excited. Furthermore the repetition rate has been investigated, in order to obtain the maximum throughput achievable with this device. In the rectangular signal case the correctness of the working has been analyzed and then comparison with the previous case is described, in terms of efficiency.

Both in continuous and pulse regime the antennas have to be placed one from the others at a distance equal to an even or odd multiple of the wavelength. Indeed the interference pattern is influenced from the phase of different inputs, but also from the distance at which exciting signals are placed.

One of the future perspective is the possibility to put the input antennas at a random position, not taking into account the wavelength. Furthermore a more deep understanding of the interference mechanisms inside the majority gate has to be achieved.

The results obtained in this master thesis give a more physical insight into the interaction among the spin waves generated by different inputs, in a majority gate structure. Promising results has been demonstrated but further studies are required to keep improving the description of the logic operation in the device. As future research goal, a full derivation of analytical equation or new models, are strongly recommended.

# Bibliography

- [1] *P. Pirro, T. Brächer, A. V. Chumak, B. Lägel, C. Dubs, O. Surzhenko, P. Görnert, B. Leven, and B. Hillebrands, "Spin-wave excitation and propagation in microstructured waveguides of yttrium iron garnet/Pt bilayers," Appl. Phys. Lett., vol. 104, p. 012402, 2014.*
- [2] *D. E. Nikonov and I. A. Young, "Benchmarking of Beyond-CMOS Exploratory Devices for Logic Integrated Circuits," IEEE Journal on Exploratory Solid-State Computational Devices and Circuits, vol. 1, pp. 3–11, 2015.*
- [3] *A. Khitun, M. Bao, and K. L. Wang, "Magnonic logic circuits," J. Phys. D: Applied Physics, vol. 43, p. 264005, 2010.*
- [4] *F. Vanderveken, "Modeling of magnetoelectric coupling for advanced spintronic applications". KU Leuven, 2018*
- [5] *R. L. Stamps, S. Breitkreutz, J. Åkerman, A. V. Chumak, Y. Otani, G. E. W. Bauer, J. Thiele, M. Bowen, S. Majetich, M. Klaui, I. J. Prejbeanu, B. Dieny, N. M. Dempsey, and B. Hillebrands, "The 2014 Magnetism Roadmap," J. Phys. D: Applied Physics, vol. 47, p. 333001, 2014.*
- [6] *D. E. Nikonov and I. A. Young, "Overview of beyond-CMOS devices and a uniform methodology for their benchmarking," Proceedings of the IEEE, vol. 101, pp. 2498–2533, 2013.*
- [7] *A. Khitun and K. L. Wang, "Nano logic circuits with spin wave bus," in Proceedings - Third International Conference on Information Technology: New Generations, ITNG 2006, 2006.*

## Bibliography

---

- [8] *A. Khitun, D. E. Nikonov, M. Bao, K. Galatsis, and K. L. Wang, "Feasibility study of logic circuits with a spin wave bus," Nanotechnology, vol. 18, p. 465202, 2007.*
- [9] *S. Klingler, P. Pirro, T. Bracher, B. Leven, B. Hillebrands, and A. V. Chumak, "Design of a spin-wave majority gate employing mode selection"*
- [10] *Florin Ciubotaru, Giacomo Talmelli, Thibaut Devolder, Odysseas Zografos, Marc Heyns, Christoph Adelmann, and Iuliana P. Radu, "First experimental demonstration of a scalable linear majority gate based on spin waves"*
- [11] *S. Chikazumi, Magnetism - From Fundamentals to Nanoscale Dynamics. New York: Oxford University Press, second ed., 1999.*
- [12] *A. Vaysset, Micromagnetic Modelling Of Spin-Transfer-Driven Magnetization Dynamics In Nanopillars. PhD thesis, Université de Grenoble, 2013.*
- [13] *F. Ciubotaru, Spin-wave excitation by nano-sized antennas. PhD thesis, Technischen Universitat Kaiserslautern, 2012.*
- [14] *C. Kittel, Introduction to solid state physics. Wiley, 1956.*
- [15] *K. Y. Guslienko, S. O. Demokritov, B. Hillebrands, and A. N. Slavin, "Effective dipolar boundary conditions for dynamic magnetization in thin magnetic stripes," Phys. Rev. B - Condensed Matter and Materials Physics, vol. 66, p. 132402, 2002.*
- [16] *B. A. Kalinikos and A. N. Slavin, "Theory of dipole-exchange spin wave spectrum for ferromagnetic films with mixed exchange boundary conditions," J. Phys C: Solid State Phys., vol. 19, pp. 7013–7033, 1986.*
- [17] *V. E. Demidov and S. O. Demokritov, "Magnonic waveguides studied by microfocus brillouin light scattering," IEEE Transactions on Magnetics, vol. 51, no. 4, p. 0800215, 2015.*
- [18] *A. A. Serga, A. V. Chumak, and B. Hillebrands, "YIG magnonics," J. Phys. D: Appl. Phys, vol. 43, p. 264002, 2010.*

## Bibliography

---

- [19] *T. Schneider, A. A. Serga, T. Neumann, B. Hillebrands, and M. P. Kostylev, "Phase reciprocity of spin-wave excitation by a microstrip antenna," Phys. Rev. B: Condensed Matter and Materials Physics, vol. 77, p. 214411, 2008.*
- [20] *T. Brächer, O. Boulle, G. Gaudin, and P. Pirro, "Creation of unidirectional spin-wave emitters by utilizing interfacial Dzyaloshinskii-Moriya interaction," Phys. Rev. B, vol. 95, p. 064429, 2017.*
- [21] *A. Conca, J. Greser, T. Sebastian, S. Klingler, B. Obry, B. Leven, and B. Hillebrands, "Low spin-wave damping in amorphous Co<sub>40</sub>Fe<sub>40</sub>B<sub>20</sub> thin films," J. Appl. Phys., vol. 113, no. 10, p. 213909, 2013.*
- [22] *A. Conca, E. Th Papaioannou, S. Klingler, J. Greser, T. Sebastian, B. Leven, J. Lösch, and B. Hillebrands, "Annealing influence on the Gilbert damping parameter and the exchange constant of CoFeB thin films," Appl. Phys. Lett., vol. 104, no. 10, p. 182407, 2014.*
- [23] *R. Duflou, Modeling of magnetoelectric and magnetoelastic coupling for advanced spintronic applications. KU Leuven, 2016.*
- [24] *Arne Vansteenkiste, Jonathan Leliaert, Mykola Dvornik, Felipe Garcia-Sanchez, and Bartel Van Waeyenberge, "The design and verification of Mumax3"*
- [25] *"Reconfigurable nanoscale spin wave majority gates with frequency-division multiplexing", Nature, 2019*
- [26] *"Excitation fluence dependence of spin-wave dynamics and intrinsic Gilbert damping in epitaxial Co<sub>2</sub>FeAl film", Japanese Journal of Applied Physics, 2019*
- [27] *D.D. Stancil and A. Prabhakar, Spin Waves Theory and Applications. Springer US, 2008.*
- [28] *S. Chikazumi, Magnetism - From Fundamentals to Nanoscale Dynamics. New York: Oxford University Press, second ed., 1999.*
- [29] *R. Duflou, Modeling of magnetoelectric and magnetoelastic coupling for advanced spintronic applications. KU Leuven, 2016.*

## Bibliography

---

- [30] *S. Chikazumi, Physics of Ferromagnetism. OUP Oxford, 2009.*